Accepted Manuscript

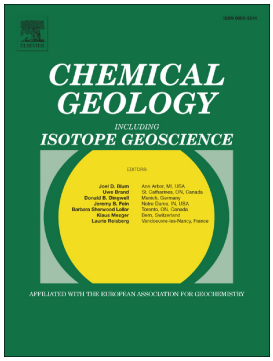

Marine redox conditions during deposition of Late Ordovician and Early Silurian organic-rich mudrocks in the Siljan ring district, central Sweden

Xinze Lu, Brian Kendall, Holly J. Stein, Chao Li, Judith L. Hannah, Gwyneth W. Gordon, Jan Ove R. Ebbestad

PII: S0009-2541(17)30140-7
DOI: doi: 10.1016/j.chemgeo.2017.03.015
Reference: CHEMGE 18283

To appear in: *Chemical Geology*

Received date: 17 August 2016
Revised date: 5 December 2016
Accepted date: 15 March 2017

Please cite this article as: Xinze Lu, Brian Kendall, Holly J. Stein, Chao Li, Judith L. Hannah, Gwyneth W. Gordon, Jan Ove R. Ebbestad , Marine redox conditions during deposition of Late Ordovician and Early Silurian organic-rich mudrocks in the Siljan ring district, central Sweden. The address for the corresponding author was captured as affiliation for all authors. Please check if appropriate. Chemge(2017), doi: 10.1016/j.chemgeo.2017.03.015

Marine redox conditions during deposition of Late Ordovician and Early Silurian organic-rich mudrocks in the Siljan ring district, central Sweden

Xinze Lu[a] *, Brian Kendall[a], Holly J. Stein[b, c], Chao Li[d] **, Judith L. Hannah[b, c], Gwyneth W. Gordon[e], Jan Ove R. Ebbestad[f]

[a] Department of Earth and Environmental Sciences, University of Waterloo, 200 University Avenue West, Waterloo, Ontario, Canada N2L 3G1

[b] AIRIE Program, Colorado State University, Fort Collins, CO 80523-1482, USA

[c] Centre for Earth Evolution and Dynamics, University of Oslo, 0315 Oslo, Norway

[d] State Key Laboratory of Biogeology and Environmental Geology, China University of Geosciences, Wuhan 430074, China

[e] School of Earth and Space Exploration, Arizona State University, Tempe, ZA 85287, USA

[f] Museum of Evolution, Uppsala University, Norbyvägen 22, SE-752 36 Uppsala, Sweden

Revised Manuscript submitted to *Chemical Geology*

December 2016

*Main corresponding author at: Department of Earth and Environmental Sciences, University of Waterloo, 200 University Avenue West, Waterloo, Ontario, Canada N2L 3G1. Email: xlv@uwaterloo.ca.

**Corresponding author for Fe speciation: chaoli@cug.edu.cn.

Abstract

The Late Ordovician Period witnessed the second largest mass extinction in the Phanerozoic Eon and the Hirnantian glaciation. To infer ocean redox conditions across the Ordovician-Silurian transition, we measured the U (as $\delta^{238}U$ relative to standard CRM145 = 0 ‰) and Mo (as $\delta^{98}Mo$ relative to standard NIST SRM 3134 = +0.25 ‰) isotope compositions of 26 organic-rich mudrock samples from the Late Ordovician (Katian) Fjäcka Shale and the Early Silurian (Aeronian-Telychian) Kallholn Formation (Siljan ring district, Sweden). The magnitude of Re, Mo, and U enrichments, Re_{EF}/Mo_{EF} and U_{EF}/Mo_{EF} ratios, and sedimentary Fe speciation point to locally euxinic bottom water conditions during deposition of the Fjäcka Shale. The same proxies suggest that black shales of the Kallholn Formation were deposited under transiently euxinic conditions with the chemocline situated near the sediment-water interface, whereas gray shales stratigraphically equivalent to the upper Kallholn Formation were deposited from oxygenated bottom waters. These observations are consistent with higher $\delta^{98}Mo$ and $\delta^{238}U$ in the Fjäcka Shale compared with the Kallholn Formation.

Because the Fjäcka Shale was deposited from persistently euxinic bottom waters, the Mo and U isotope compositions from these rocks can be used to estimate the extent of global ocean euxinia and ocean anoxia (euxinic plus ferruginous conditions), respectively. Elevated Mo_{EF} and Mo/TOC ratios in the euxinic Fjäcka Shale suggest no more than moderate basin restriction from the open ocean as well as non-quantitative removal of Mo from the euxinic bottom waters, thus pointing to Mo isotope fractionation between seawater and the euxinic sediments. Hence, we infer that even the highest $\delta^{98}Mo$ (+1.28 ‰) preserved in the Fjäcka Shale is only a minimum estimate for the Mo isotope

composition of coeval global seawater. Correcting for seawater-sediment Mo isotope fractionation, the δ^{98}Mo of late Katian seawater may have been +1.4–2.1 ‰, which corresponds to ~10–70% Mo removal into the euxinic sink. The average authigenic δ^{238}U of the Fjäcka Shale is –0.05 ‰ to +0.02 ‰ after correcting for a range of possible detrital δ^{238}U values, thus yielding an overall average of ~0 ‰. Taking into account isotope fractionation during U removal to euxinic sediments, we infer that late Katian seawater δ^{238}U was about –0.85 ‰ to –0.60 ‰. A steady-state U isotope mass balance model reveals that 46−63% of riverine U input was removed in anoxic settings. Based on the Mo and U isotope data, we infer that euxinic and anoxic waters may have covered < 1% and at least 5% (potentially tens of percent) of the total seafloor area during the late Katian, respectively, based on previously published models that relate the magnitude of Mo and U burial fluxes to the areal extent of euxinic and anoxic seafloor. By comparison, only 0.21−0.35% and < 1% of the total seafloor area was covered by anoxic waters today and during the Cenozoic, respectively. The difference between the estimated extent of ocean anoxia (euxinic plus ferruginous) and ocean euxinia points to an appreciable extent of ferruginous water masses during the late Katian. Integration of our data with previous studies thus supports the hypothesis that ocean oxygenation intensified during the subsequent Hirnantian glaciation (when seawater δ^{98}Mo temporarily reached values similar to today). Hence, environmental stresses related to glaciation, not an expansion of ocean anoxia, may have triggered the first phase of the Hirnantian mass extinction.

Keywords: uranium isotopes; molybdenum isotopes; Katian; Hirnantian glaciation; euxinic; ferruginous

1. INTRODUCTION

The environmental conditions of the Ordovician world (485-444 Ma) played an important role in metazoan evolution, extinction, and biogeographic distribution. Relatively high sea-level stands (Haq and Schutter, 2008), a pronounced greenhouse climate state for most of the period (Shields et al., 2003), paleocontinents mostly located in the Southern Hemisphere (Cocks and Torsvik, 2002, 2005), probable superplume events (e.g., Huff et al., 1996; Bergström et al., 2004; Christidis and Huff, 2009), and a terminal Ordovician (Hirnantian) glaciation (e.g., Brenchley et al., 2003; Saltzman and Young, 2005; Delabroye et al., 2010) were the key features of the Ordovician Earth. Notable biological events at this time include rapid biota diversification (the Great Ordovician Biodiversification Event; GOBE) in the early Middle Ordovician (e.g., Webby et al., 2004; Servais et al., 2009) and the second largest Phanerozoic extinction event in the Late Ordovician, with ~85% loss of species (Brenchley et al., 2001; Sheehan, 2001). Recovery of biodiversity to pre-extinction levels (similar to the early Middle Ordovician) by surviving species and communities required at least 4-5 Myr (Brenchley et al., 2001; Sheehan, 2001).

The nature of ocean redox conditions before, during, and after a two-phase mass extinction event and associated glaciation in the Hirnantian has been a subject of recent debate. The Hirnantian glaciation ended the pronounced greenhouse environment of the preceding Ordovician, and resulted in rapid cooling and eustatic fall (Fig. 1; Finnegan et al., 2011). Rapid cooling may have been the major kill mechanism for the first extinction phase during the early to middle Hirnantian (Brenchley et al., 2001; Melchin et al., 2013).

Associated with the Hirnantian glaciation is a strong positive $\delta^{13}C$ excursion (HICE: Hirnantian Isotope Carbon Excursion) (Fig. 1; e.g., Marshall and Middleton, 1990; Brenchley et al., 1994; Kump et al., 1999; Webby et al., 2004; Bergström et al., 2006; LaPorte et al., 2009; Ainsaar et al., 2010; Zhou et al., 2015) that can be explained by either increased burial of organic carbon (Brenchley et al., 1994; Hammarlund et al., 2012; Zhou et al., 2015), or the exposure and weathering of carbonate platforms (with high $\delta^{13}C$) in low latitudes due to eustatic fall (Kump et al., 1999). Evidence for increased ocean oxygenation and potentially more vigorous ocean circulation in response to glaciation was suggested based on a switch from deposition of black shales to gray shales (Brenchley, 1989; Finney et al., 1999; LaPorte et al., 2009; Melchin et al., 2013). Hammarlund et al. (2012) suggested instead that positive pyrite $\delta^{34}S$ and organic carbon $\delta^{13}C$ excursions at this time reflect an expansion of water column euxinia that, together with sea-level fall, was responsible for the first phase of the Hirnantian mass extinction. The second phase of the mass extinction occurred during the middle-late Hirnantian, and is thought to be associated with expansion of ocean anoxia following the demise of the glaciation (Brenchley et al., 2001; Melchin et al., 2013), or expansion of euxinic waters onto shallower continental shelves because of sea-level rise (Hammarlund et al., 2012). Quantifying the extent of ocean anoxia and euxinia during the Hirnantian and the preceding Katian can help resolve these competing hypotheses.

Recently, the stable Mo isotope system was used to infer global ocean redox conditions across the Ordovician-Silurian transition (Dahl et al., 2010a; Zhou et al., 2012, 2015). Removal of dissolved Mo from seawater to sediments is strongly tied to the availability of dissolved sulfide in the water column and sediment pore fluids, such that

high, moderate, and low Mo enrichments are found in sediments deposited in euxinic, suboxic to anoxic/non-sulfidic (ferruginous), and well-oxygenated marine environments, respectively (Morford and Emerson, 1999; McManus et al., 2006; Kendall et al., 2010; Scott and Lyons, 2012; Reinhard et al., 2013). The Mo isotope composition of organic-rich mudrocks (ORMs) deposited from strongly euxinic bottom waters ($[H_2S]_{aq}$ > 11 μM) may directly capture the global seawater Mo isotope composition, particularly in restricted basins where Mo removal from bottom waters is quantitative (Barling et al., 2001; Arnold et al., 2004; Neubert et al., 2008). However, ORMs deposited from non-euxinic or weakly euxinic bottom waters ($[H_2S]_{aq}$ < 11 μM) have variably lower δ^{98}Mo than global seawater, reflecting the preferential removal of lighter Mo isotopes to sediments in these environments (Arnold et al., 2004; Neubert et al., 2008; Gordon et al., 2009; Poulson Brucker et al., 2009). Hence, the Mo isotope paleoredox proxy is most sensitive to the areal extent of euxinic versus non-euxinic marine environments.

Temporal compilations of Mo isotope data from euxinic ORM suggest that the δ^{98}Mo of global seawater between 520 and 440 Ma was typically ~+1.0−1.4 ‰, with one instance of higher values (+2.4 ‰) in the early Hirnantian associated with glaciation (Dahl et al., 2010a; Zhou et al., 2012, 2015; Kendall et al., 2015). The consistently low seawater δ^{98}Mo values during 520−440 Ma compared with today (+2.34 ± 0.10 ‰; Barling et al., 2001; Siebert et al., 2003; Nakagawa et al., 2012; Nägler et al., 2014) potentially suggest that the oceans were generally less oxygenated and contained a greater extent of water column euxinia, consistent with generally lower Mo concentrations in euxinic ORM deposited at this time compared with later Phanerozoic ORM (Dahl et al., 2010a; Zhou et al., 2012, 2015; Kendall et al., 2015). However, local

redox proxies such as Fe speciation and Mo enrichments cannot quantitatively reveal whether ORMs were deposited from weakly versus strongly euxinic bottom waters. Hence, it remains possible that significant Mo isotope fractionation occurred between seawater and euxinic sediments in some cases. It is therefore possible that the extent of ocean oxygenation during the Ordovician and Silurian has been generally underestimated. In addition, Zhou et al. (2015) suggested that stratigraphic variations in the Mo isotope data of Ordovician-Silurian ORM from the Yangtze Platform (South China) were primarily influenced by changes in local rather than global ocean redox conditions.

Because the Mo isotope proxy is more sensitive to the extent of ocean euxinia rather than general ocean anoxia (i.e., euxinic plus ferruginous conditions; Neubert et al., 2008; Cheng et al., 2015), new global ocean paleoredox proxies are needed to test hypotheses regarding the extent of ocean oxygenation at the Ordovician-Silurian transition. The U isotope system in ORMs represents an emerging global ocean paleoredox proxy with good potential to provide constraints on the extent of general ocean anoxia because U burial in anoxic sediments is primarily mediated by both microbial Fe(III) reduction and microbial sulfate reduction, and thus is less dependent on H_2S availability compared with Mo (e.g., Morford and Emerson, 1999; Weyer et al., 2008; Montoya-Pino et al., 2010; Asael et al., 2013; Partin et al., 2013; Basu et al., 2014; Stirling et al., 2015; Stylo et al., 2015; Kendall et al., 2015). Notably, consistently large experimental U isotope fractionations are observed during the microbially mediated reduction of U(VI) to U(IV) by several different bacterial strains (Basu et al., 2014; Stirling et al., 2015; Stylo et al., 2015). The greatest extent of U isotope fractionation in the marine environment occurs in anoxic settings (where the heavier ^{238}U isotope is

preferentially removed to sediments) whereas distinctly smaller U isotope fractionations occur in oxygenated and suboxic environments (e.g., Weyer et al., 2008; Montoya-Pinos et al., 2010; Brennecka et al., 2011b; Andersen et al., 2014; Holmden et al., 2015; Noordmann et al., 2015). Hence, the combined use of the U and Mo isotope systems gives a more robust approach for inferring global ocean redox conditions than the Mo isotope system alone by shedding insight on the areal extent of both euxinic and ferruginous conditions (Asael et al., 2013; Kendall et al., 2015). In this study, sedimentary Fe speciation data, trace metal concentrations, and U and Mo isotope data are reported for ORMs deposited before and after the Hirnantian in the Siljan ring district, central Sweden.

2. GEOLOGICAL BACKGROUND

The Siljan ring district (61.04°N, 14.92°E; Fig. 2) is located in central Sweden, and is thought to be the largest impact structure in Europe (present-day diameter of 52 km, and an estimated ~90 km diameter before erosion; Grieve, 1988; Holm et al., 2011; Juhlin et al., 2012). Recently, the Siljan ring has been a focus of research under the project "Concentric Impact Structures in the Paleozoic" (CISP; Högström et al., 2010), which is one of the essential parts of the "Swedish Deep Drilling Program" (SDDP; Lorenz et al., 2010) (Fig. 2). Since 2011, three additional holes (Mora 001, Solberga #1, and Stumsnäs #1) in the Siljan area were drilled and cored by the Swedish private company IGRENE AB for geothermal energy and natural gas exploration.

The Siljan region was part of Baltica, which was situated at equatorial latitudes during the Late Ordovician (Cocks and Torsvik, 2002, 2005). At that time, the depositional environment in the Siljan area was a shallow marine continental shelf (Cocks and Torsvik, 2005). Stratigraphic studies show that the basin deepened to the west (Larson et al., 1999; Cederbom et al., 2000). Subsequently, the Scandinavian Caledonides developed on collision between Baltica and Laurentia during the Late Silurian to Early Devonian (Cederbom et al., 2000; Huigen and Andriessen, 2004). Sedimentary rocks in the Oslo area, south Norway, record the associated Caledonian foreland basin (Huigen and Andriessen, 2004).

The Siljan structure is thought to have been caused by the Devonian impact of a meteorite on a seabed underlain by sedimentary rocks of Ordovician and Silurian age. Evidence for a bolide impact origin includes planar deformation structures in quartz (Tamminen and Wickman, 1980), occurrence of shatter cones (Svensson, 1973), and fluid inclusion analyses (Komor et al., 1988). New $^{40}Ar/^{39}Ar$ laser spot data and step-heating data for a melt breccia indicate an impact age of 380.9 ± 4.6 Ma (Reimold et al., 2005; Jourdan et al., 2012). Precambrian bedrock is exposed in this ring-like depression, particularly in the 30-km-wide central plateau (Fig. 2). Around the impact margins, jostled blocks of Ordovician and Silurian strata are exposed, providing an opportunity to study the regional Early Paleozoic sedimentary sequences and paleoenvironments (Ebbestad and Högström, 2007; Lehnert et al., 2012, 2013). These Early Paleozoic sedimentary rocks are unmetamorphosed and well preserved.

The basal Tremadocian Obolus beds of Ordovician age are the oldest in the preserved Paleozoic lithostratigraphic succession, whereas the Nederberga Formation

shales of Middle Silurian age mark the top of the succession (Grahn, 1998; Ebbestad and Högström, 2007). The Ordovician stratigraphy is similar to that observed in other parts of Sweden (e.g., Ebbestad and Högström, 2007; Lehnert et al., 2012). The regional geological succession and lithostratigraphy are summarized by Ebbestad and Högström (2007). More recently, a geological correlation of the terminal Ordovician succession based on carbon isotope stratigraphy and biostratigraphy from five quarries and eight sections was presented by Ebbestad et al. (2014) (Fig. 3). Biostratigraphic ages in the Siljan ring district are based on well-characterized biozones (Ebbestad and Högström, 2007; Ebbestad et al., 2014).

Petroleum was produced from organic-rich source rocks as a result of the Siljan impact event rather than by deep burial, as indicated by biomarker thermal maturity indicators in the source rocks. Oil-source rock correlation analysis using biomarkers and carbon isotope data indicate that the Siljan ring oil was sourced predominantly from the Ordovician Fjäcka Shale (formally "*Tretaspis* shale"), probably with a minor contribution from the Silurian Kallholn Formation (formally "*Rastrites* shale") (Vlierboom et al., 1986; Ahmed et al., 2014). Stein et al. (2009, 2014) reported a four-point Re-Os age of 812 ± 48 Ma for heavy oil recovered from seeps penetrating the Katian Boda limestone in the Solberga quarry. The four oil samples have constant Re (1.4−1.6 µg/kg) but highly variable Os concentrations (40−300 ng/kg) that are interpreted as mixtures of meteoritic debris and oil (Stein et al., 2014). The initial $^{187}Os/^{188}Os$ (0.20 ± 0.12) from the Re-Os regression indicates an unradiogenic extraterrestrial contribution to the oils. Although the Re-Os isotope system in oil was significantly disturbed by inclusion of meteoritic material during hydrocarbon formation, there is no evidence of similar isotopic

disturbance to the shales (Stein et al., 2009, 2014). Hence, geochemical data from the Fjäcka Shale and Kallholn Formation in the Siljan ring can be used to reconstruct Late Ordovician and Early Silurian ocean redox conditions.

The Fjäcka Shale is the main focus of this study and was deposited during the late Katian, broadly coeval with the "Boda Event" (Fortey and Cocks, 2005; Cherns and Wheeley, 2007). The early-middle part of the Late Ordovician (Sandbian and Katian stages) was characterized by sea levels that were generally 100−200 m higher than today (Haq and Schutter, 2008; Fig. 1). Sea surface temperature (SST) variations, based on clumped oxygen isotope data from carbonates and oxygen isotope data from conodont apatite, show a general cooling trend during this time (Trotter et al., 2008; Finnegan et al., 2011; Fig. 1). This cooling trend may have been briefly interrupted in the late Katian by the warmer "Boda Event" based on migrations of benthic species from low to high latitude and the occurrence of warm water near the South Pole (Fortey and Cocks, 2005), which is also suggested by SST variation profiles (Fig. 1; Finnegan et al., 2011; Melchin et al., 2013). However, Cherns and Wheeley (2007) alternatively considered the "Boda Event" to mark global cooling based on detailed facies analysis.

For this study, 26 samples were obtained from the Mora 001, Solberga #1, and Stumsnäs #1 drill cores. Lithostratigraphic units and detailed core descriptions are reported in Lehnert et al. (2012, 2013). Upper Ordovician rock units are preserved in the eastern (Solberga #1) and southern (Stumsnäs #1) Siljan ring. However, Late Ordovician stratigraphy is absent in Mora 001 from the western Siljan ring, which has been explained by movement of the Caledonian peripheral forebulge from west to east (Lehnert et al., 2012). Six samples of Early Silurian light gray shale were obtained from a "lower shale

member" that has a thickness of about 62 m in Mora 001. Based on new graptolite findings, the gray shale (early Telychian) is broadly equivalent to the upper Kallholn Formation (Aeronian-Telychian) (Lehnert et al., 2013). In Solberga #1, the thickness of the Kallholn Formation and Fjäcka Shale is 60 m and 6 m, respectively. Four samples of the Kallholn Formation and six samples of the Fjäcka Shale were obtained from Solberga #1. In Stumsnäs #1, the Fjäcka Shale has a thickness of 5 m and 10 samples were obtained from this drill core. The samples were selected from intervals previously collected for Re-Os isotope studies (Stein et al., 2009, 2014).

3. PROXIES AND ANALYTICAL METHODS

3.1. Sedimentary iron speciation

Sedimentary Fe speciation has been widely used to evaluate local bottom water redox conditions for paleoenvironmental studies (e.g., Poulton and Raiswell, 2002; Anderson and Raiswell, 2004; Poulton et al., 2004, 2010; Lyons and Severmann, 2006; Canfield et al., 2008; Li et al., 2010; Reinhard et al., 2009; Kendall et al., 2010, 2015; Poulton and Canfield, 2011). Biogeochemically highly reactive iron (Fe_{HR}) can react with sulfide in the water column or in sediments during early diagenesis, and is mainly composed of pyrite Fe (Fe_{py}), carbonate Fe (Fe_{carb}), ferric oxide Fe (Fe_{ox}), and magnetite Fe (Fe_{mag}), such that $Fe_{HR} = Fe_{carb} + Fe_{ox} + Fe_{mag} + Fe_{py}$ (Poulton and Canfield, 2005). Total Fe (Fe_T) consists of unreactive or poorly reactive Fe mainly associated with silicate minerals and the aforementioned highly reactive Fe species (Poulton et al., 2004).

The ratio of Fe_{HR}/Fe_T in modern sediments and Phanerozoic sedimentary rocks is usually < 0.38 for oxygenated marine settings (Raiswell and Canfield, 1998; Poulton and Raiswell, 2002), whereas higher ratios predominantly indicate anoxic bottom waters. Analyses of Phanerozoic sediments and sedimentary rocks suggest that 0.22 is a reasonable lower limit to distinguish oxic from anoxic conditions in bottom waters (Poulton and Raiswell, 2002; Poulton and Canfield, 2011). Hence, Fe_{HR}/Fe_T can be used to distinguish anoxic (≥ 0.38) from oxic (≤ 0.22) conditions. However, it is noted that low Fe_{HR}/Fe_T can represent a false signature for oxic conditions if Fe precipitation from an anoxic water column is inefficient, sedimentation rates were rapid, or Fe remobilization occurred during diagenesis (Planavsky et al., 2011; Poulton and Canfield, 2011; Sperling et al., 2015). Other indicators such as redox-sensitive trace metal enrichments (e.g., Re, Mo, U) should therefore be used to confirm an oxic signature derived from Fe speciation (e.g., Kendall et al., 2010). In anoxic environments , ferruginous and euxinic conditions can be distinguished by using the extent of pyritization of the highly reactive iron pool (Fe_{py}/Fe_{HR}). Values of $Fe_{py}/Fe_{HR} > 0.7$ indicate euxinic conditions, whereas values < 0.7 indicate ferruginous conditions (März et al., 2008; Poulton and Canfield, 2011).

Sedimentary Fe speciation analyses were performed at the State Key Laboratory of Biogeology and Environmental Geology, China University of Geoscience (Wuhan). A sequential extraction method (described in Poulton and Canfield, 2005) and atomic absorption spectroscopy (AAS) was used for obtaining Fe_{carb}, Fe_{ox}, and Fe_{mag} contents, with a relative standard deviation (RSD) of less than 5% (Li et al., 2015). Sulfide was extracted and measured using a modified chromium reduction method (Canfield et al., 1986), and Fe_{py} content was then calculated based on a pyrite mineral formula of FeS_2 (Li

et al., 2015). Recovery rates for pyrite extraction, as tested on a pure pyrite standard (Alfa Aesar) for two batches, are both > 92%. Since no international standards for sequential extraction of Fe species have been established, two internal laboratory standards (CUG-2, CUG-3) have been repeatedly used and tested in the Lyons Biogeochemistry Laboratory at the University of California, Riverside (UCR). Our average values of Fe_{carb}, Fe_{ox}, and Fe_{mag} from CUG-2 are 0.13 ± 0.02% (1SD, n=7), 0.21 ± 0.02% (1SD, n=7), and 0.11 ± 0.01% (1SD, n=7), which are in excellent agreement with average values for Fe_{carb} (0.11%), Fe_{ox} (0.20%), and Fe_{mag} (0.10%) measured at UCR. Our average values of Fe_{carb}, Fe_{ox}, and Fe_{mag} from CUG-3 are 1.21 ± 0.14% (1SD, n=4), 0.21 ± 0.02% (1SD, n=4), and 0.52 ± 0.10% (1SD, n=4), which also match the average values for Fe_{carb} (1.26%), Fe_{ox} (0.20%), and Fe_{mag} (0.64%) measured at UCR.

3.2. Elemental analyses

Trace element concentrations and U and Mo isotope compositions (see Section 3.3 and 3.4) were measured at the W.M. Keck Foundation Laboratory for Environmental Biogeochemistry, School of Earth and Space Exploration, Arizona State University (ASU). Samples were powdered in a ball mill using silicon nitride jars. Splits of the powdered samples were ashed at 550°C overnight (to oxidize organic matter) and dissolved in concentrated HF–HNO_3–HCl. A weighed split of each sample solution was diluted with 0.32M HNO_3 and element concentrations were analyzed using a Thermo i-CAP quadrupole inductively coupled plasma mass spectrometer (Q-ICP-MS). A split of powder from the USGS Devonian Ohio Shale standard SDO-1 was dissolved and

analyzed along with samples to verify instrument accuracy. Trace element concentration reproducibility was within 10%.

To evaluate local redox conditions during deposition of the studied stratigraphic units, the enrichment factors (EFs) of U, Mo, and Re were calculated relative to average upper crust. The EF is calculated as follows (Tribovillard et al., 2006):

$$EF = [metal / Al]_{sample} / [metal / Al]_{average\ upper\ crust}$$

The average upper crust data for U (2.8 mg/kg), Mo (1.5 mg/kg), and Al (8.04 wt.%) are from McLennan (2001), and Re (1.0 μg/kg) is from Selby et al. (2007).

Total organic carbon (TOC) contents were analyzed by Activation Laboratories Ltd. The TOC is calculated by the difference between total carbon (TC) and total inorganic carbon (TIC). The TC was analyzed on an ELTRA CS 2000 Carbon Sulphur Analyzer. A split of the sample powder was weighed and combusted at 1370°C in a nearly pure oxygen environment. After removal of moisture and dust, the resulting CO_2 released by combustion was measured using a solid-state infrared detector for TC. A separate split of sample powder was dissolved by 20% HCl, enabling the amount of TIC to be quantified using the same measurement procedure as described above. This procedure results in a detection limit of 0.5 wt.% for TOC content.

3.3. Uranium isotopes

Uranium isotope measurements followed the experimental procedures stated in Weyer et al. (2008) and Kendall et al. (2013). A weighed amount of double spike solution (^{233}U and ^{236}U) was added to a split of each digested sample solution to correct for column chromatography and instrument mass bias. Eichrom® UTEVA resin was used to

isolate and purify U from sample solutions. Uranium isotope measurements were performed on a Thermo Scientific Neptune multiple collector (MC) ICP-MS instrument using an ESI Apex desolvating nebulizer. The U isotope ratio ($\delta^{238}U$) of each sample was reported relative to the CRM145 standard:

$$\delta^{238}U_{\text{ sample}}\,(‰) = (^{238/235}U_{\text{ sample}} / {}^{238/235}U_{\text{ CRM145}} - 1) \times 1000$$

Repeated measurements of the U isotope standards CRM145 (measured against itself) and CRM129a yielded average $\delta^{238}U$ of 0.00 ± 0.09 ‰ (2SD, n=87) and –1.70 ± 0.10 ‰ (2SD, n=8), respectively. The average value for CRM129a is statistically identical to that reported by earlier studies (Brennecka et al., 2011a; Kendall et al., 2013, 2015). During the course of this study, the SDO-1 standard was also analyzed and yielded an average $\delta^{238}U$ of –0.11 ± 0.10 ‰ (2SD, n=3), which is in agreement with the average of –0.06 ± 0.04 ‰ (2SD, n=17) reported for SDO-1 by Kendall et al. (2015). The 2SD uncertainty of a sample is reported as the 2SD uncertainty of sample replicate measurements or 0.09 ‰ (the average uncertainty of CRM145, CRM129a, and SDO-1), whichever is greater.

3.4. Molybdenum isotopes

Measurement of Mo isotope compositions followed the protocols stated in Duan et al. (2010) and Herrmann et al. (2012). A weighed amount of double spike (^{97}Mo and ^{100}Mo) was added to a split of each digested sample solution to correct for mass bias. Subsequently, the purification of Mo was carried out by a two-step column chemistry procedure that involved first anion and then cation exchange chromatography (Barling et al., 2001; Arnold et al., 2004; Duan et al., 2010). Molybdenum isotope analysis was

performed on the Neptune MC-ICP-MS instrument using an ESI Apex desolvating nebulizer.

Molybdenum isotope data for samples are first measured relative to an in-house standard (RochMo2) and then are re-calculated relative to the new international NIST SRM 3134 standard (Nägler et al., 2014). Thus, Mo isotope data are reported as follows (Nägler et al., 2014):

$$\delta^{98}Mo_{\ sample}\ (‰) = 1000 \times [(^{98}Mo/^{95}Mo)_{sample}/(^{98}Mo/^{95}Mo)_{NIST\ SRM\ 3134}) - 1] + 0.25$$

By setting the δ^{98}Mo of NIST SRM 3134 to +0.25 ‰, the δ^{98}Mo of open ocean seawater is +2.34 ± 0.10 ‰ (2SD) (Goldberg et al., 2013; Nägler et al., 2014), which is statistically identical (given analytical uncertainties) to the seawater value (~+2.3 ‰) previously measured against many in-house standards in different laboratories (Barling et al., 2001; Siebert et al., 2003; Arnold et al., 2004; Nakagawa et al., 2012). In this way, the "traditional" seawater δ^{98}Mo value of ~+2.3 ‰ can be kept and Mo isotope data measured relative to in-house standards in most laboratories can now be directly compared after re-normalizing to NIST SRM 3134 (Goldberg et al., 2013; Nägler et al., 2014).

The NIST SRM 3134 standard has a heavier Mo isotope composition (+0.33 ± 0.05 ‰; 2SD, n=99) compared with the in-house RochMo2 standard at ASU (Goldberg et al., 2013). In this study, the measured value for NIST SRM 3134 was +0.31 ± 0.04 ‰ (2SD, n=10) relative to RochMo2. Hence, 0.06 ‰ was subtracted from each sample Mo isotope composition measured relative to RochMo2 so that all data is reported relative to NIST SRM 3134 = +0.25 ‰. The average δ^{98}Mo for SDO-1 in this study was +1.06 ± 0.05 ‰ and +0.81 ± 0.05 ‰ (2SD, n=13) relative to NIST SRM 3134 = +0.25 ‰ and 0.00 ‰, respectively. The latter value is in excellent agreement with the average δ^{98}Mo

values for SDO-1 of +0.80 ± 0.14 ‰ (2SD, n=504) reported by Goldberg et al. (2013) for multiple laboratories, and +0.82 ± 0.11 ‰ (2SD, n=145) reported by Goldberg et al. (2013) for double spike analyses using the ASU Neptune MC-ICP-MS. Given the average uncertainty of SDO-1, we report the 2SD uncertainty of a sample as the 2SD uncertainty of sample replicate measurements or 0.11 ‰, whichever is greater.

4. RESULTS

4.1. TOC contents, iron speciation, and trace metal enrichments

The Fjäcka Shale contains high TOC contents (4.0−8.2 wt.%) with an average of 5.6 wt.% (Table 1 and Fig. 4). Consistently high ratios of Fe_{HR}/Fe_T (> 0.38) and Fe_{py}/Fe_{HR} (> 0.79) (Fig. 5), together with high trace metal enrichments (U_{EF}: 5.5−10.1; Mo_{EF}: 14.2−214.4; Re_{EF}: 33.2−108.1) (Table 1), are observed for the Fjäcka Shale at both the Stumsnäs #1 and Solberga #1 localities (Figs. 6–7).

Black shales from the Kallholn Formation in drillcore Solberga #1 have relatively lower TOC contents of 2.9 to 6.5 wt.% (average = 4.2 wt.%) compared with the Fjäcka Shale (Table 1, Figs. 4, 6). Lower trace metal EFs are observed in the Kallholn Formation black shales compared with the Fjäcka Shale (Fig. 7). The sample at 61.46 m has lower trace metal enrichments (U_{EF}: 4.1; Mo_{EF}: 3.1; Re_{EF}: 9.2) and lower Fe speciation ratios (Fe_{HR}/Fe_T = 0.28; Fe_{py}/Fe_{HR} = 0.79) compared with other Kallholn Formation black shales (U_{EF}: 4.2−6.7; Mo_{EF}: 10.1−32.7; Re_{EF}: 11.0−55.1; $Fe_{HR}/Fe_T \geq 0.34$; $Fe_{py}/Fe_{HR} \geq 0.86$) (Table 1, Figs. 4–5).

The gray shales in drill core Mora 001 have the lowest TOC contents (≤ 1.0 wt.%) and are also characterized by low Fe_{HR}/Fe_T (0.19−0.24) and Fe_{py}/Fe_{HR} (0.47−0.60) ratios and low trace metal enrichments (U_{EF}: 1.4−2.7; Mo_{EF}: 1.5−5.7; Re_{EF}: 1.3−13.4) (Table 1, Figs. 4–7).

4.2. Uranium and molybdenum isotope compositions

The $\delta^{238}U$ and $\delta^{98}Mo$ of the Fjäcka Shale range from −0.24 ‰ to +0.10 ‰ and from +0.42 ‰ to +1.28 ‰, respectively (Table 1). The middle Fjäcka Shale in Stumsnäs #1 has the highest Mo_{EF} (> 103), U_{EF} (> 8), and Re_{EF} (> 68), and the highest $\delta^{238}U$ (+0.01 ‰ to +0.10 ‰) and $\delta^{98}Mo$ (+0.92 ‰ to +1.28 ‰). Overlying and underlying shales in this drillcore exhibit relatively lower $\delta^{238}U$ (top: −0.17 ‰ to +0.01 ‰; bottom: −0.08 ‰ to +0.03 ‰) and lower $\delta^{98}Mo$ (top: +0.58 ‰ to +1.09 ‰; bottom: +0.63 ‰ to +1.28 ‰). No obvious stratigraphic trend is observed for the Fjäcka Shale in Solberga #1 (Fig. 4).

The black shales of the Kallholn Formation in Solberga #1 yield generally lower $\delta^{238}U$ (−0.34 ‰ to −0.10 ‰) and $\delta^{98}Mo$ (+0.44 ‰ to +0.86 ‰) compared with the Fjäcka Shale. A similar observation can be made for the two gray shales of the uppermost Kallholn Formation ($\delta^{238}U$: −0.29 ‰ to −0.07 ‰; $\delta^{98}Mo$: +0.40 ‰ to +0.48 ‰) (Table 1).

In the Fjäcka Shale, the $\delta^{98}Mo$ values are moderately correlated with Mo_{EF} (R^2 = 0.61, n=21, p(α) < 0.0001), whereas the Kallholn Formation black and gray shales display no correlation (R^2 = 0.05, n=7, p(α) = 0.6298) (Fig. 8a). Only a weak positive correlation between $\delta^{238}U$ and U_{EF} is observed for the Fjäcka Shale (R^2 = 0.25, n=19, p(α)

= 0.0293), and no correlation is observed for the Kallholn Formation black and gray shales (R^2 = 0.08, n=6, p(α) = 0.5871) (Fig. 8b).

5. DISCUSSION

5.1. Local marine redox conditions

Shales deposited from locally euxinic bottom waters contain pronounced authigenic enrichments of redox-sensitive metals and are an attractive target for estimating global ocean redox conditions using Mo and U concentrations and isotope compositions (e.g., Gordon et al., 2009; Montoya-Pino et al., 2010). Consistently high ratios of Fe_{HR}/Fe_T (> 0.38) and Fe_{py}/Fe_{HR} (> 0.79) as well as high Mo_{EF}, Re_{EF}, and U_{EF} indicate that the Fjäcka Shale was deposited from persistently euxinic bottom waters (Figs. 5, 7).

On the contrary, the gray shales equivalent to the upper Kallholn Formation were likely deposited from oxygenated bottom waters, asindicated by low TOC contents and low Fe_{HR}/Fe_T ratios of 0.19−0.24. Since Re enrichment in sediments occurs under anoxic conditions with or without the presence of dissolved H_2S whereas Mo removal from sediment pore waters requires dissolved H_2S (i.e., more intensely reducing conditions), the relative enrichments of Mo_{EF} and Re_{EF} in sediments can be further used to indicate the depth of O_2 penetration into sediments (Morford and Emerson, 1999; Morford et al., 2005). Some gray shales have small Mo_{EF} accompanied by stronger Re_{EF}, suggesting O_2 penetration was < 1 cm below the sediment-water interface (Morford and Emerson, 1999; Morford et al., 2005). Other gray shales have low Re_{EF} and Mo_{EF}, suggesting a greater

depth of O_2 penetration (> 1 cm) into sediments that enables Re, U, and Mo diffusion from sediment pore waters back into the water column. Hence, the U and Mo isotope compositions of the grey shales are not suitable for inferring global ocean redox conditions.

The more TOC-rich black shales of the Kallholn Formation were probably deposited under both non-euxinic and euxinic bottom water conditions. Weakly oxygenated conditions may be represented by sample 61.46 m, which has a low Fe_{HR}/Fe_T ratio (0.28) and low Mo (3.1) and Re (9.2) enrichments, although we cannot exclude the possibility of anoxic and ferruginous conditions. By comparison, the other Kallholn Formation black shales were likely deposited under euxinic waters based on their higher Fe_{HR}/Fe_T ratios (0.34−0.58), consistently high Fe_{py}/Fe_{HR} (> 0.80) ratios, and elevated trace metal enrichments (Fig. 4). These observations suggest that the position of the chemocline fluctuated and was close to the sediment-water interface during deposition of the Kallholn Formation black shales. A switch from euxinic conditions to oxygenated conditions can cause re-mobilization and re-deposition of redox-sensitive trace metals at deeper depths within sediments, thus obscuring the original depositional trends (Morford and Emerson, 1999; Morford et al., 2005). Hence, we conclude that the black shales of the Kallholn Formation may not be suitable for inferring global ocean redox conditions by using Mo-U isotopes.

Because the Fjäcka Shale was deposited from persistently euxinic bottom waters, it is the main focus of our efforts to infer global ocean redox conditions in the following discussion. In the Fjäcka Shale, the correlation between Mo and TOC is poor (R^2 = 0.04, n=18, p(α) = 0.4262), as is the correlation between U and TOC contents (R^2 = 0.16, n=18,

p(α) = 0.1000) (Fig. 6). The weak correlation between U and TOC contents is not unexpected for ORMs deposited under euxinic conditions because U may not be directly associated with organic matter in ORMs but rather can be found in authigenic phases like UO_2 (Algeo and Maynard, 2004; Tribovillard et al., 2006). However, the poor correlation between Mo and TOC contents was not expected because strong Mo-TOC correlations are commonly observed for sediments deposited in modern euxinic basins (Algeo and Lyons, 2006; Georgiev et al., 2011). By contrast, Re and TOC contents are well-correlated in the Fjäcka Shale (R^2 = 0.93 if sample 135.01 m is excluded, n=17, p(α) < 0.0001), clearly indicating a hydrogenous origin for Re (e.g., Anbar et al., 2007). The reason for the poor Mo-TOC correlation in the Fjäcka Shale is not known, but may be related to water chemistry (e.g., pH; Helz et al., 2011) or to multiple host phases for Mo (e.g., both organic matter and sulfide minerals; Chappaz et al., 2014) rather than post-depositional disturbance (Ardakani et al., 2016) given that a good Re-TOC correlation and minimal open-system Re-Os isotope behavior was observed for these ORMs (Stein et al., 2009, 2014).

Low Mo/TOC ratios and low Mo_{EF}/U_{EF} ratios in euxinic sediments are observed in strongly restricted basins like the Black Sea due to highly efficient removal of Mo to sediments and slow Mo recharge rates from the open ocean (Algeo and Lyons, 2006; Algeo and Tribovillard, 2009). Neither feature is observed in the Fjäcka Shale. Although Mo/TOC ratios of the Fjäcka Shale vary widely (average: 13.5 mg/kg/wt.%), most are intermediate between that of modern euxinic sediments in the Saanich Inlet (~45 mg/kg/wt.%) and Black Sea (~4.5 mg/kg/wt.%) (Algeo and Lyons, 2006), suggesting no more than moderate basin restriction during Fjäcka Shale deposition (Fig. 6a; particularly

if the global oceanic Mo reservoir during the late Katian was lower than the modern ocean, which would cause lower Mo/TOC ratios in ORM). This interpretation is consistent with Mo/U ratios of the Fjäcka Shale. High Mo_{EF}/U_{EF} ratios (average = 5.1) in the Fjäcka Shale, which in some cases exceed three times the modern seawater molar Mo/U ratio, can be explained by more efficient removal of Mo to euxinic sediments compared with U, but without significant drawdown of seawater Mo concentrations (Fig. 7a; Algeo and Tribovillard, 2009). These interpretations are consistent with the Mo_{EF}/Re_{EF} ratios (average = 1.7) of the Fjäcka Shale, which are broadly similar to the molar Mo/Re ratio of modern seawater (Fig. 7b).

The ORMs of the Fjäcka Shale in Solberga #1 and Stumsnäs #1 have some similarities and differences in geochemical characteristics (Table 2). Significant overlap in the TOC contents, Fe speciation ratios, and Re_{EF} is observed between the two drillcores, and there is no meaningful statistical difference between the drillcore averages (based on unpaired t-tests). The Fe speciation ratios indicate euxinic conditions for the Fjäcka Shale at both the Solberga #1 and Stumsnäs #1 localities, but this technique is not capable of precisely quantifying the H_2S levels of euxinic waters and thus cannot be used to determine if the two localities had strongly ($[H_2S]_{aq}$ > 11 μM) or weakly ($[H_2S]_{aq}$ < 11 μM) euxinic bottom waters. Distinctly higher Mo_{EF} (and to a lesser extent U_{EF}) are observed in Stumsnäs #1, suggesting more strongly euxinic bottom water conditions at this locality. Hence, the ORMs from Stumsnäs #1 may be the most suitable for inferring global ocean redox conditions using Mo isotopes. Indeed, higher δ^{98}Mo is observed in the Fjäcka shale in the Stumsnäs #1 core. Although higher δ^{238}U is also observed in Stumsnäs #1, the δ^{238}U of modern euxinic sediments does not appear dependent on the

amount of H_2S in bottom waters, unlike $\delta^{98}Mo$ (Neubert et al., 2008; Andersen et al., 2014; Holmden et al., 2015). Possibly, this explains the moderate correlation between Mo_{EF} and $\delta^{98}Mo$, but poor correlation between U_{EF} and $\delta^{238}U$ in the Fjäcka Shale (see Section 4.2).

5.2. Uranium isotope constraints on the extent of anoxia in the late Katian ocean

5.2.1. The U isotope paleoredox proxy

Uranium is primarily derived from the oxidative weathering of continental crust, and subsequent transport of dissolved U(VI) by rivers to the oceans (Morford and Emerson, 1999; Dunk et al., 2002; Partin et al., 2013). In modern oxygenated seawater, U is highly soluble and mainly exists as uranyl carbonate ($UO_2[CO_3]_3^{4-}$; Langmuir, 1978), with a long residence time (~ 400−500 kyr) in the oceans (Ku et al., 1977; Dunk et al., 2002). In contrast, soluble U(VI) is reduced to insoluble U(IV) below the sediment-water interface, primarily because of microbial Fe(III) and sulfate reduction (abiotic reduction of U is kinetically slower), resulting in removal of U from anoxic pore waters into organic matter, sulfide minerals, and authigenic U phases (e.g., uraninite) (Anderson, 1987; Anderson et al., 1989; Barnes and Cochran, 1990; Morford and Emerson, 1999; McManus et al., 2006; Tribovillard et al., 2006; Asael et al., 2013; Partin et al., 2013). Biogenic carbonates, sediments deposited from anoxic and suboxic waters, and coastal zones are major sinks for U. Sediments deposited from well-oxygenated waters and hydrothermally altered oceanic crust are minor U sinks (Morford and Emerson, 1999; Dunk et al., 2002; Partin et al., 2013; Noordmann et al., 2015; Tissot and Dauphas, 2015; Andersen et al., 2016; Wang et al., 2016).

The U isotope system is a promising ocean paleoredox proxy that has been applied to carbonates (Brennecka et al., 2011a; Romaniello et al., 2013; Chen et al., 2016), Fe-Mn crusts (Goto et al., 2014; Noordmann et al., 2016; Wang et al., 2016), and ORMs (Weyer et al., 2008; Montoya-Pino et al., 2010; Asael et al., 2013; Kendall et al., 2013, 2015). Modern well-oxygenated seawater has a $\delta^{238}U$ of −0.39 ± 0.01 ‰ (Stirling et al., 2007; Weyer et al., 2008; Tissot and Dauphas, 2015; Andersen et al., 2016; Noordmann et al., 2016). The average $\delta^{238}U$ of the upper crust (−0.29 ± 0.04 ‰; Tissot and Dauphas, 2015; Noordmann et al., 2016) is slightly higher than that of modern seawater by ~+0.1 ‰. The range of average $\delta^{238}U$ values suggested for rivers (–0.27 ‰ to –0.34 ‰) is similar to average upper crust, implying minor U isotope fractionation ($\Delta^{238}U_{sediment-SW}$) during weathering and river transport (Stirling et al., 2007; Tissot and Dauphas, 2015; Andersen et al., 2016; Noordmann et al., 2016). Minor U sources to seawater such as groundwater and aeolian inputs are poorly constrained (Dunk et al., 2002; Tissot and Dauphas, 2015).

In anoxic environments, a large, volume-dependent, U isotope fractionation accompanies the reduction and precipitation of U, resulting in preferential removal of the heavier ^{238}U isotope from seawater to sediments (Biegeleisen, 1996; Schauble, 2007; Stirling et al., 2007; Weyer et al., 2008; Montoya-Pino et al., 2010; Andersen et al., 2014; Noordmann et al., 2015). Recent ORMs from Black Sea Unit I, deposited from strongly euxinic waters ($H_2S_{(aq)}$ > 11 μM), have an average $\delta^{238}U$ value of +0.03 ± 0.20 ‰ (Weyer et al., 2008; Montoya-Pino et al., 2010), which is about +0.4 ‰ higher compared with that of modern global seawater. However, the magnitude of U isotope fractionation observed in the Black Sea can only be regarded as a minimum value because the Black

Sea is a strongly restricted basin (Anderson et al., 1989) and partial U depletion (~40%) in the deep waters has occurred due to U burial in sediments coupled with slow rates of deep water renewal (Andersen et al., 2014). Similar logic applies to the Kyllaren fjord, Norway (Noordmann et al., 2015). A U isotope fractionation factor of ~+0.62 ± 0.17 ‰ (2σ) between global seawater and authigenic U in euxinic sediments was observed for the more open ocean Saanich Inlet, Canada (Holmden et al., 2015). This larger isotope fractionation is more similar to that observed during microbially-mediated U reduction (+0.68 ‰ to +0.99 ‰; average ~ +0.85 ‰), which may be the main process responsible for U removal to sediments (Basu et al., 2014; Stirling et al., 2015; Stylo et al., 2015). Hence, the representative U isotope fractionation between modern seawater and open ocean euxinic sediments may be about +0.60 ‰ to +0.85 ‰. Previous U isotope paleoredox studies assumed a fractionation of only ~+0.5−0.6 ‰ (e.g., Montoya-Pino et al., 2010; Brennecka et al., 2011a; Kendall et al., 2015).

The magnitude of U isotope fractionation is smaller in other marine sinks. Sediments from the Peru continental margin overlying suboxic bottom waters have slightly higher $\delta^{238}U$ (−0.28 ± 0.19 ‰) than modern seawater (Weyer et al., 2008). The Fe-Mn crusts from the Pacific ocean overlying well-oxygenated bottom waters have an average $\delta^{238}U$ value of −0.65 ± 0.05 ‰ (Goto et al., 2014) to −0.61 ± 0.09 ‰ (Wang et al., 2016). Hence, Fe-Mn crusts are offset by about –0.25 ‰ from seawater, consistent with experimental observations (Brennecka et al., 2011b). Primary carbonate precipitates have an average $\delta^{238}U$ (−0.37 ± 0.12 ‰) that is indistinguishable from global seawater regardless of biological or mineralogical origin (Romaniello et al., 2013), consistent with minor to negligible isotope fractionation during co-precipitation of U with calcite and

aragonite (Chen et al., 2016). However, the $\delta^{238}U$ of shallow bulk carbonates that contain dissolved H_2S in pore waters exhibit a U isotope fractionation of +0.2−0.4 ‰ compared with that of modern seawater (Romaniello et al., 2013). Low-temperature hydrothermal alteration of oceanic basalts may be associated with a net U isotope fractionation of about +0.25 ‰, favoring removal of the heavier ^{238}U isotope into altered basalts (Andersen et al., 2015; Tissot and Dauphas, 2015; Noordmann et al., 2016). The magnitude of U isotope fractionation in coastal retention zones (due to U uptake by oxide minerals and organic matter) may be around −0.24 ‰, although more work needs to be done to confirm this value (Tissot and Dauphas, 2015).

Based on this modern framework, an expansion of ocean anoxia will increase the extent of preferential removal of isotopically heavier U from seawater to anoxic sediments, thus resulting in lighter $\delta^{238}U$ for global seawater (Weyer et al., 2008; Montoya-Pino et al., 2010; Brennecka et al., 2011a). Therefore, ancient ORMs deposited during times of more expanded ocean anoxia compared with today will take on a lower $\delta^{238}U$ signature as seawater $\delta^{238}U$ shifts to lower values.

5.2.2. Uranium isotope composition of the late Katian ocean

Given the moderate authigenic U enrichments in the Fjäcka Shale (U_{EF} = 5.5–10.1), the bulk $\delta^{238}U$ in these rocks were influenced to a minor extent by detrital minerals, thus requiring calculation of authigenic $\delta^{238}U$. Holmden et al. (2015) proposed that detrital $\delta^{238}U$ may have a much lower value (−0.83 ± 0.12 ‰) in Saanich Inlet sediments compared with the average upper crust as a result of preferential release of ^{238}U into solution during weathering. However, Tissot and Dauphas (2015) and Andersen et al.

(2016) suggested limited overall U isotope fractionation between the upper continental crust and rivers as a result of weathering. Nevertheless, because local variations in the $\delta^{238}U$ of detrital material are possible, a range of detrital $\delta^{238}U$ (−0.8 ‰ to −0.3 ‰) is reasonable to use for calculating the proportion and isotopic composition of authigenic U in the Fjäcka Shale. Calculation of the authigenic $\delta^{238}U$ can be done using the following equation (Asael et al., 2013):

$$\delta^{238}U_a = \delta^{238}U_s - (Al/U)_s \times \{(\delta^{238}U_d - \delta^{238}U_s) / [(Al/U)_d - (Al/U)_s]\}$$

where “a”, "s", and "d" represent authigenic U, sample U, and detrital U, respectively. Detrital Al and U concentrations are assumed to be the average upper continental crust values of 8.04 wt.% and 2.8 mg/kg, respectively (McLennan, 2001).

The average authigenic $\delta^{238}U$ of the Fjäcka Shale for both drillcores is −0.05 ± 0.11 ‰ (1SD) and +0.02 ± 0.11 ‰ (1SD) when using detrital $\delta^{238}U$ values of −0.3 ‰ and −0.8 ‰, respectively. After correction, it is found that the detrital component comprises up to 15% of the U in the Fjäcka Shale. Although Stumsnäs #1 may represent the more euxinic site during deposition of the Fjäcka Shale based on the higher Mo enrichments at that locality, the $\delta^{238}U$ of euxinic ORMs is not thought to depend on the amount of aqueous H_2S in the water column (Andersen et al., 2014; Holmden et al., 2015). Hence, we report an overall average authigenic $\delta^{238}U$ of ~0 ‰ for both drillcores (Table 3).

Applying the U isotope fractionation between global seawater and open ocean euxinic sediments (+0.60 ‰ to +0.85 ‰) to the average authigenic $\delta^{238}U$ of the Fjäcka Shale (~0 ‰), we suggest that the $\delta^{238}U$ of the late Katian ocean was approximately −0.60 ‰ to −0.85 ‰, which is lower than the modern well-oxygenated ocean (–0.4 ‰). Hence, the late Katian ocean was characterized by a greater extent of anoxia compared

with today. We now use a simple U isotope mass-balance model to quantify the extent of anoxia.

5.2.3. Quantitative constraints on the extent of anoxia in the late Katian ocean

5.2.3.1. Uranium isotope mass balance in the modern ocean

Uranium isotope mass balance modeling can be used to obtain a first-order estimate of the extent of anoxic conditions in the late Katian ocean. This method has been used to constrain the extent of ocean anoxia during the Cretaceous Oceanic Anoxic Event 2 (OAE2) (Montoya-Pino et al., 2010) and the end-Permian mass extinction event (Brennecka et al., 2011a). The U isotope mass balance equation is defined below (Montoya-Pino et al., 2010):

$$\delta^{238}U_{input} = (f_{anox} \times \delta^{238}U_{anox}) + (f_{other} \times \delta^{238}U_{other}),$$

where "input" = riverine U inputs, "anox" = anoxic and euxinic U sinks, "other" = all other U sinks (suboxic, carbonates, Fe-Mn oxides, oceanic crust alteration including high temperature [HT] and low temperature [LT], pelagic clays, coastal), "f" = the fraction of U removed into each corresponding sink, and $f_{other} + f_{anox} = 1$.

The average $\delta^{238}U$ of the input is assumed to be equivalent to the riverine average of approximately −0.3 ‰ (Tissot and Dauphas, 2015; Andersen et al., 2016; Noordmann et al., 2016) given that aeolian and groundwater inputs are small and poorly characterized. An overall fractionation factor (+0.043 ‰) between the "other" sinks and modern seawater can be calculated as the weighted average of those individual sinks in the modern ocean, suggesting an average $\delta^{238}U$ of −0.357 ‰ for the "other" sinks (Andersen et al., 2014, 2016; Tissot and Dauphas, 2015; Wang et al., 2016; Noordmann et al., 2016;

Table 4). Applying a fractionation factor of +0.60 ‰ to +0.85 ‰ between global seawater and anoxic/euxinic sediments, a $\delta^{238}U$ range of +0.20 ‰ to +0.45 ‰ is assumed for the modern anoxic/euxinic sink. Applying these values to the U isotope mass balance equation and assuming steady-state conditions, 7−10% of the riverine U flux is removed into the anoxic/euxinic sink. Therefore, other sinks represent 90-93% of the U removal flux (Fig. 9A).

5.2.3.2. Uranium isotope mass balance in the late Katian ocean

The U isotope mass balance equation can be used to estimate the proportion of U that was removed into the anoxic sink in the late Katian using the modern mass balance as a starting point (Montoya-Pino et al., 2010; Brennecka et al., 2011a). As described previously, late Katian seawater $\delta^{238}U$ may have been –0.60 ‰ to –0.85 ‰ based on the average authigenic $\delta^{238}U$ of the Fjäcka Shale (~0 ‰; assumed to be representative of the anoxic/euxinic sink at this time). The $\delta^{238}U$ of late Katian rivers is assumed to be similar to the modern value (–0.3 ‰) since the eroding upper continental crust today and during the late Katian probably had a similar U isotope composition (e.g., Andersen et al., 2015; Dhuime et al., 2015; Tang et al., 2016). It is assumed that U isotope fractionations between seawater and the two defined sinks were similar for the late Katian and modern oceans. Hence, when late Katian seawater = –0.60 ‰, then the $\delta^{238}U$ of the anoxic/euxinic sink and all other sinks are 0 ‰ (= –0.60 ‰ + 0.60 ‰) and –0.557 ‰ (= –0.60 ‰ + 0.043 ‰), respectively. When late Katian seawater = –0.85 ‰, then the $\delta^{238}U$ of the anoxic/euxinic sink and all other sinks are 0‰ (= –0.85 ‰ + 0.85 ‰) and –0.807 ‰ (= –0.85 ‰ + 0.043 ‰), respectively.

Based on these estimates for the U isotope composition of the two sinks, we calculate that the anoxic/euxinic U sink and the other U sinks in the late Katian ocean constitute 46−63% and 37−54%, respectively, of the total U sink flux (Fig. 9B). According to the U isotope mass balance model, the proportion of U removed to anoxic/euxinic sinks in the late Katian ocean may have been approximately four to nine times larger compared with that of the modern ocean, thus indicating a greater extent of late Katian ocean anoxia compared with modern well-oxygenated ocean. Applying the same logic and calculation method (a simple steady-state U isotope mass balance model with two sinks and a U isotope fractionation of +0.60−0.85 ‰ between seawater and the anoxic/euxinic sink) to other U isotope studies, we provide new estimates for the proportions of U removed into the anoxic/euxinic sink during the OAE2, late Permian, and late Ediacaran (Table 5). These calculations show that the size of the anoxic/euxinic U sink during the late Katian overlaps with estimates for OAE2 and the late Permian, and was significantly higher compared with the late Ediacaran and today.

5.3. Marine redox conditions during the late Katian as inferred from Mo isotopes

5.3.1. The Mo isotope paleoredox proxy

Dissolved Mo in seawater is mainly derived from oxidative weathering of the upper crust and transportation of soluble molybdate (MoO_4^{2-}) by rivers to the oceans. Molybdenum behaves conservatively in oxygenated seawater and has a long residence time of 440 kyr (Miller et al., 2011). In anoxic settings, Mo becomes insoluble and is removed into sediments, especially in the presence of dissolved sulfide (e.g., Emerson and Huested, 1991; Helz et al., 1996, 2011; Erickson and Helz, 2000; Scott et al., 2008;

Scott and Lyons, 2012). Intermediate thiomolybdate ions (e.g., $MoO_{4-x}S_x^{2-}$) are the dominant species if the $H_2S_{(aq)}$ concentration is low, whereas tetrathiomolybdate (MoS_4^{2-}) and to a lesser extent trithiomolybdate ($MoOS_3^{2-}$) occurs when $H_2S_{(aq)}$ is > ~11 μM (Erickson and Helz, 2000; Nägler et al., 2011). Reactions with zero-valent sulfur are suggested to form particle-reactive Mo polysulfides that are sequestered by organic matter and solid Fe-S phases (Helz et al., 1996, 2011; Erickson and Helz, 2000; Tribovillard et al., 2004, 2006; Algeo and Lyons, 2006; Dahl et al., 2013; Chappaz et al., 2014).

The Mo isotope system in ORM has been used widely over the past 12 years to reconstruct global ocean paleoredox conditions (e.g., Arnold et al., 2004; Siebert et al., 2005; Wille et al., 2007, 2008; Pearce et al., 2008, 2010; Gordon et al., 2009; Kendall et al., 2009, 2011, 2015; Dahl et al., 2010a, 2011; Duan et al., 2010; Dickson and Cohen, 2012; Dickson et al., 2012; Herrmann et al., 2012; Zhou et al., 2012, 2015; Asael et al., 2013; Proemse et al., 2013; Westermann et al., 2014; Chen et al., 2015; Kurzweil et al., 2015). The modern ocean has a δ^{98}Mo of +2.34 ± 0.10 ‰ (Barling et al., 2001; Siebert et al., 2003; Nakagawa et al., 2012; Nägler et al., 2014) that is significantly higher than rivers (average = +0.7 ‰; Archer and Vance, 2008). This difference in isotopic composition between the rivers and oceans arises from the preferential removal of lighter Mo isotopes in sediments, which is most pronounced in oxygenated settings.

In well-oxygenated ocean sediments, lighter Mo isotopes preferentially adsorb to Fe-Mn oxides and crusts, resulting in an equilibrium isotope fractionation of ~3 ‰ and an average δ^{98}Mo for Fe-Mn oxides and crusts of around –0.7 ‰ (Barling et al., 2001; Siebert et al., 2003; Poulson et al., 2006; Poulson Brucker et al., 2009). In contrast, a

much smaller Mo isotope fractionation (0.7 ‰) is observed in continental margin ORMs deposited in weakly oxygenated and anoxic environments ($O_2 \leq 10$ μM) where H_2S is restricted to the sediment pore waters, resulting in sediments with a δ^{98}Mo of ~+1.6 ‰ (Poulson et al., 2006; Siebert et al., 2006; Poulson Brucker et al., 2009; Goldberg et al., 2012). More intermediate redox environments are characterized by a range of intermediate δ^{98}Mo that reflects the relative importance of Fe versus Mn oxide formation in the water column and subsequent reductive dissolution of these oxides in sediments and complexing of Mo with dissolved sulfide from sediment pore waters (Siebert et al., 2006; Poulson Brucker et al., 2009; Goldberg et al., 2009, 2012). Specifically, Mn-rich and Fe-rich sediments with low dissolved porewater H_2S have δ^{98}Mo of –1.0 ‰ to +0.4 ‰ and –0.5 ‰ to +2.0 ‰, respectively (Siebert et al., 2006; Goldberg et al., 2009, 2012).

In a strongly euxinic environment ($H_2S_{(aq)} \geq 11$ μM) with slow recharge of Mo to deep waters (i.e., restricted marine basin or lakes), molybdate is rapidly transformed to trithiomolybdate and tetrathiomolybdate and subsequently to Mo polysulfide species, and removed nearly quantitatively from bottom waters to sediments, as observed in the modern Black Sea, Kyllaren fjord, and Lake Cadagno, Switzerland (Neubert et al., 2008; Dahl et al., 2010b, 2013; Noordmann et al., 2015). In this scenario, global seawater δ^{98}Mo is directly captured by the euxinic sediments, despite the pronounced basin restriction, because of the long oceanic residence time of Mo (Barling et al., 2001; Arnold et al., 2004; Neubert et al., 2008; Noordmann et al., 2015). Based on Black Sea measurements, a minor Mo isotope fractionation of 0.5 ± 0.3 ‰ may occur between dissolved trithiomolybdate or tetrathiomolybdate and authigenic solid-phase Mo in sediments if there is incomplete removal of Mo from strongly euxinic bottom waters

(Nägler et al., 2011). The δ^{98}Mo of organic-rich sediments in weakly euxinic environments ($H_2S_{(aq)}$ < 11 µM) is known to display a much larger range of Mo isotope fractionation (up to ~3 ‰), which may be caused by incomplete conversion of molybdate to the highly reactive trithiomolybdate and tetrathiomolybdate species (each reaction step in the conversion of molybdate to tetrathiomolybdate is associated with Mo isotope fractionation) or periodic flushing of the basin with O_2-rich waters (Arnold et al., 2004; Nägler et al., 2005; Tossell, 2005; Neubert et al., 2008; Nägler et al., 2011; Noordmann et al., 2015).

Based on these modern observations, a more oxygenated ocean should have a higher δ^{98}Mo than a more anoxic ocean because a generally smaller extent of Mo isotope fractionation occurs between seawater and sediments under anoxic conditions (and especially under strongly euxinic conditions), thus limiting the increase of seawater δ^{98}Mo over the river baseline. The δ^{98}Mo of strongly euxinic ORMs has the best potential of all ORM to record the global seawater δ^{98}Mo during deposition and thus capture direct information about the extent of global ocean euxinia (because Mo burial is extremely efficient in euxinic settings; Arnold et al., 2004; Neubert et al., 2008; Scott et al., 2008).

5.3.2. Extent of late Katian ocean euxinia

The more euxinic Fjäcka Shale from Stumsnäs #1 (based on Mo enrichments) has a higher average δ^{98}Mo (+0.91 ± 0.26 ‰; 1SD) compared with Solberga #1 (+0.62 ± 0.12 ‰; 1SD) (Table 2; detrital Mo represents < 5% of the Mo budget for each sample, so no correction for detrital Mo was made). The highest δ^{98}Mo of +1.24−1.28 ‰ occurs in samples 219.74 m, 219.95 m, and 220.87 m from Stumsnäs #1, which have high Mo_{EF}

(62−214) and Mo/TOC ratios (11−37 mg/kg/wt.%), suggesting these samples are most likely to mimic seawater δ^{98}Mo during deposition (e.g., Arnold et al., 2004; Gordon et al., 2009; Dahl et al., 2010a). However, the high Mo enrichments indicate that Mo removal from bottom waters was probably not quantitative and thus even these highest δ^{98}Mo values are probably only minimum estimates for coeval seawater.

High Mo_{EF}/U_{EF} ratios for the Fjäcka Shale, in some cases exceeding three times the modern seawater molar Mo/U ratio, indicate the potential operation of an Fe-Mn particulate shuttle (Fig. 7a) (Algeo and Tribovillard, 2009). The particulate shuttle can enrich sediments in isotopically light Mo through reductive dissolution of Mo-bearing Fe-Mn oxides in sediments and recapture of the Mo by sulfides and organic matter (e.g., Herrmann et al., 2012; Scholz et al., 2013; Cheng et al., 2016). In this scenario, the Fjäcka Shale samples with the highest Mo_{EF}/U_{EF} ratios should generally have lower δ^{98}Mo than samples with lower Mo_{EF}/U_{EF} ratios. However, the samples with the highest δ^{98}Mo have high Mo_{EF}/U_{EF} ratios, implying that a particulate shuttle did not significantly influence the δ^{98}Mo of the Fjäcka Shale. In addition, a steep slope of $(Mo_{EF}/U_{EF})_{auth}$ is typically observed with operation of a particulate shuttle in modern anoxic basins (Algeo and Tribovillard, 2009), but this is not observed for the Fjäcka Shale (Fig. 7a). A moderate positive correlation is observed between Mo enrichments and δ^{98}Mo for the Fjäcka Shale. These observations collectively suggest that dissolved sulfide levels in the water column rather than an Fe-Mn particulate shuttle influenced the Mo systematics in these rocks (Fig. 8a).

Although high Mo enrichments and Fe speciation can fingerprint local euxinic bottom water conditions, these proxies cannot reveal whether bottom water $H_2S_{(aq)}$ was

high enough for quantitative conversion of molybdate to tetrathiomolybdate and Mo polysulfide species. It is thus possible that Mo isotope fractionation between seawater and the Fjäcka Shale occurred as a result of deposition from weakly euxinic bottom waters. The modern Cariaco Basin and shallower parts of the Black Sea (near the chemocline) both contain weakly euxinic bottom waters ($H_2S_{(aq)} < 11$ μM) but the sediments in these two locations have distinctly different ranges in δ^{98}Mo (+1.5 ‰ to +2.2 ‰, and –0.6 ‰ to +0.9 ‰, respectively; Arnold et al., 2004; Neubert et al., 2008). The reasons for the different δ^{98}Mo in these two weakly euxinic settings are poorly understood. If the Fjäcka Shale is analogous to the deep Cariaco Basin (i.e., deep-water deposition and more similar extent of basin restriction), then applying the observed Mo isotope fractionations of 0.1−0.8 ‰ characterizing the deep Cariaco Basin to the heaviest δ^{98}Mo in the Fjäcka Shale suggests that late Katian seawater δ^{98}Mo was between +1.4 ‰ and +2.1 ‰.

It is also possible that the Fjäcka Shale was deposited in a strongly euxinic setting such that Mo isotope fractionation resulted solely from non-quantitative removal of Mo from the bottom waters. A 0.5 ± 0.3 ‰ fractionation between strongly euxinic bottom waters and sediments may occur when there is quantitative conversion of all intermediate thiomolybdates to trithiomolybdates or tetrathiomolybdates but incomplete removal of Mo from the bottom waters into sediments (we note that this fractionation factor was estimated for the Black Sea and has yet to be verified in other modern anoxic basins; Nägler et al., 2011). If this situation applies to the Fjäcka Shale, then late Katian seawater δ^{98}Mo should be ~+1.5−2.1 ‰, which is similar to the estimate derived for the assumption of Cariaco-style weakly euxinic conditions.

In both cases (weakly or strongly euxinic), the inferred late Katian seawater δ^{98}Mo (between +1.4 ‰ and +2.1 ‰) is lower than the modern ocean, indicating a greater extent of euxinia compared with today. For this range of seawater δ^{98}Mo, between about 10% and 70% of the riverine Mo flux could have been removed into the euxinic sink, as calculated by Chen et al. (2015) assuming steady-state conditions and a three sink (oxic, suboxic, and euxinic) mass balance model for Mo.

5.4. Implications for Late Ordovician ocean redox conditions and the first phase of the Hirnantian mass extinction

The global seawater δ^{238}U and δ^{98}Mo inferred for the late Katian can be used to infer the areal extent of general ocean anoxia and euxinia, respectively. Mass balance models have been developed by recent studies to relate the magnitude of Mo and U burial fluxes into sediments of different redox character (and the associated isotope fractionations for each redox setting) to the areal extent of seafloor covered by those sinks (Dahl et al., 2011; Reinhard et al., 2013; Chen et al., 2015; Wang et al., 2016), and we used the results of mass balance modelling shown in the tables and figures from these studies to get our estimates. The mass balance models are tailored to the specific redox geochemistry of each metal. Based on the Mo concentration of the euxinic Fjäcka Shale and our estimate of late Katian seawater δ^{98}Mo, the actual area of seafloor covered by euxinic waters was probably < 1% of the total seafloor (compared with < 0.2% today; Dahl et al., 2011; Reinhard et al., 2013, Chen et al., 2015). By comparison, the estimated late Katian seawater δ^{238}U suggests that general ocean anoxia (both euxinic and ferruginous conditions) covered at least 5% (potentially tens of percent; precise estimates

are not possible given large uncertainties in U isotope fractionation factors for the anoxic and suboxic sinks) of the total seafloor (compared with 0.21−0.35% today and <1% during the Cenozoic Era), based on the model of Wang et al. (2016).

The significant difference in the extent of seafloor covered by euxinic waters (as inferred from Mo isotopes) and anoxic waters (euxinic plus ferruginous; as inferred from U isotopes) points to an appreciable extent of anoxic and ferruginous water masses in the late Katian ocean. This finding is consistent with Fe speciation evidence for ferruginous water masses at some times and places in the oceans during the early Paleozoic (Cambrian to Devonian; Sperling et al., 2015). A greater extent of weakly/mildly oxygenated waters potentially also accompanied this larger extent of ocean anoxia during the late Katian, in which case the areal extent of strongly oxygenated deep waters beneath which Fe-Mn oxides were permanently buried was significantly lower than today (Reinhard et al., 2013; Chen et al., 2015; Wang et al., 2016). Our study highlights that the combined application of the Mo and U isotope paleoredox proxies has good potential to significantly improve constraints on the global extent and spatiotemporal variation of euxinic and ferruginous ocean redox conditions during the early Paleozoic, which is important for understanding the transition to generally widespread ocean oxygenation and its impact on biogeochemical cycles and metazoan evolution. Because the seawater residence times of Mo and U should be substantially higher than ocean mixing times even at significant extents of ocean anoxia (e.g., Dahl et al., 2011), the coupled Mo-U isotope approach may better constrain the global extent of ferruginous versus euxinic waters compared with Fe speciation, which is strictly a local redox proxy.

A small number of samples of early Hirnantian ORM from South China have δ^{98}Mo that is similar to modern seawater δ^{98}Mo (Zhou et al., 2012, 2015). Most of these samples also have high Mo_{EF} (> 200) that suggest deposition from locally euxinic bottom waters in a moderately restricted basin that had sufficient access to a large dissolved Mo reservoir (Scott and Lyons, 2012). This combination of high Mo enrichment and high δ^{98}Mo points to widespread ocean oxygenation since mass balance constraints dictate that only this redox state permits both a large global oceanic Mo reservoir and high seawater δ^{98}Mo (Scott et al., 2008; Dahl et al., 2010b; Reinhard et al., 2013; Chen et al., 2015; Kendall et al., 2015). We agree with Zhou et al. (2015) that the high δ^{98}Mo from the early Hirnantian ORM may reflect intensification of local euxinia but advocate that the high δ^{98}Mo also requires a well-oxygenated global redox state (other samples with lower δ^{98}Mo may simply reflect non-euxinic conditions or lower bottom water $[H_2S]_{aq}$). Hence, we re-interpret the Mo isotope data from the South China ORM together with the Mo and U isotope data from the Fjäcka Shale in central Sweden as evidence for an increase in ocean oxygenation from the late Katian to early Hirnantian in response to glaciation. The Hirnantian glaciation would have lowered ocean temperatures, thus increasing the solubility of O_2 in seawater, and decreased the nutrient supply to the oceans via reduced rates of continental weathering. Global cooling likely increased the temperature gradient between the equatorial and polar areas, thus causing increased wind-driven mixing of ocean waters. Together these factors promoted increased ocean oxygenation and therefore the reduction of O_2-depleted deeper waters (LaPorte et al., 2009).

Positive excursions in $\delta^{34}S_{py}$, $\delta^{34}S_{sulfate}$, $\delta^{13}C_{carb}$, and $\delta^{13}C_{org}$ during the early-mid Hirnantian have been explained by increases in pyrite and organic matter burial, thus

supporting expanded ocean anoxia as a mechanism for the first extinction pulse (e.g., Marshall and Middleton, 1990; Brenchley et al., 1994; Zhang et al., 2009; Hammarlund et al., 2012). However, the carbon and sulfur isotope records of early-mid Hirnantian sections are not always coupled, and it has been shown that positive S isotope excursions in the Phanerozoic rock record do not consistently point to increased ocean anoxia (Melchin et al., 2013). Interpretation of sulfur isotope trends in the context of ocean redox conditions can be complicated, for example, by diagenetic effects or changes in the microbial sulfur cycle and associated sulfur isotope fractionations (Zhang et al., 2011; Jones and Fike, 2013; Melchin et al., 2013). Hence, a sulfidic driver for the first extinction pulse during the early-mid Hirnantian (Hammarlund et al., 2012) is not fully supported by the light stable isotope data. Instead of interpreting HICE as the result of increased organic carbon burial, an alternative explanation is weathering of exposed carbonate platforms during eustatic fall triggered by Hirnantian glaciation (Kump et al. 1999; Melchin and Holmden, 2006). This interpretation is compatible with the Mo isotope evidence for extensive ocean oxygenation during the early Hirnantian.

Increased ocean oxygenation between the late Katian and early-mid Hirnantian is consistent with other geological and geochemical data. Low nitrogen isotope compositions ($\delta^{15}N = -1$ ‰ to +1 ‰) in sediments deposited in the late Katian and at the Hirnantian-Rhuddanian (Ordovician-Silurian) boundary suggest that deep oceans during these times were relatively depleted of fixed nitrogen, resulting in a deficiency of nitrogen returning to the photic zone via oceanic upwelling (LaPorte et al., 2009; Melchin et al., 2013). Hence, the $\delta^{15}N$ data are consistent with our U and Mo isotope evidence for less extensive ocean oxygenation compared with today. Higher $\delta^{15}N$ during the early-mid

Hirnantian (+2−4 ‰) suggests less intense denitrification and a greater extent of oxygenation in the deep oceans (LaPorte et al., 2009; Melchin et al., 2013), consistent with the highest δ^{98}Mo observed in Hirnantian ORM (Zhou et al., 2012, 2015). Similarly, the proportion of ORM intervals deposited from oxic/suboxic versus anoxic bottom waters based on geochemical data (δ^{34}S, trace element concentrations) was greater during the early-mid Hirnantian compared with the late Katian and early Rhuddanian (Melchin et al., 2013). Re-interpretation of the early Hirnantian Mo isotope data as representing widespread ocean oxygenation can be further tested by applying the U isotope paleoredox proxy to Hirnantian ORM.

Climate conditions during the late Ordovician have been simulated by several general circulation models (e.g., Herrmann et al., 2004; Pohl et al., 2016). The advanced FOAM (Fast Ocean Atmosphere Model), which is coupled with climate and ice sheet feedback processes, shows that the accumulation of ice sheets may have occurred in two distinct phases (Pohl et al., 2016). When atmospheric CO_2 dropped from 16 PAL to 12 PAL (present atmospheric level), which corresponds to a drop of ~1.3°C in the tropical SST (Trotter et al., 2008), ice sheets abruptly occurred and expanded from the South Pole (> 60°S) to the middle latitudes (45°S) (Pohl et al., 2016). Combined with SSTs from Trotter et al. (2008), the climate models suggest that the first ice sheet occurrence was as early as the late Darriwilian (Middle Ordovician) (Herrmann et al., 2004; Pohl et al., 2016). The second modeled ice sheet accumulation is more severe and occurs in the early Hirnantian when atmospheric CO_2 dropped from 8 PAL to 3 PAL (Pohl et al., 2016). The expanded ice sheet reached low-latitudes (30°S) (Pohl et al., 2016), and was associated with a strong positive carbon isotope excursion (e.g., Bergström et al. 2009), eustatic fall

(Haq and Schutter, 2008), and significant global cooling (a drop of ~7°C in tropical SST, more severe temperature drops probably occurred on land) (Trotter et al., 2008). Hence, the first ice sheet occurrence during the late Middle Ordovician was likely a response of general cooling, and this process was sufficiently mild that it did not cause severe environmental changes. However, the second ice sheet expansion during the early-middle Ordovician was more rapid, and thus had a more significant influence on environmental changes, biogeochemical cycles, and metazoans.

Therefore, rapid global cooling is suggested to be the major killing mechanism for the first extinction phase during the early-middle Hirnantian, which is consistent with the biomarker record (e.g., a significant decline in trilobites and brachiopods; Brenchley et al., 2001). Rapid environmental change, loss of shallow-marine and epicontinental habitats due to sea-level fall, and changes in nutrient cycles may have been significant ecological stresses associated with the glaciation. Even increased oxygenation was a stressor for some organisms, notably graptolites, who would have lost their preferred habitats in the denitrification zones at sites of high primary productivity (Melchin et al., 2013, and references therein). Increased ocean oxygenation from the late Katian to the early-middle Hirnantian, as inferred from paleoredox data (U and Mo isotopes; Zhou et al., 2012, 2015; this study), geological data (black versus gray shale distribution; Melchin et al., 2013) and geochemical data (N isotopes; Laporte et al., 2009; Melchin et al., 2013) collectively argues against expanded ocean anoxia as the trigger for the first pulse of the Hirnantian mass extinction.

6. CONCLUSIONS

A combination of Fe speciation, Mo-U-Re enrichments, and Mo_{EF}/U_{EF} and Mo_{EF}/Re_{EF} ratios constrain local bottom water redox conditions during deposition of the Late Ordovician and Early Silurian ORMs in the Siljan ring district, central Sweden. These records indicate a euxinic depositional environment for the Fjäcka Shale, fluctuations between euxinic and non-euxinic conditions for black shales of the Kallholn Formation, and an oxygenated setting for gray shales equivalent to the upper Kallholn Formation.

New U isotope data (−0.05 ‰ to +0.02 ‰; average of ~0‰) from the euxinic Fjäcka Shale suggest that late Katian seawater $\delta^{238}U$ was between –0.60 ‰ and –0.85 ‰. Uranium isotope mass balance modeling suggests that the magnitude of U burial into the anoxic sink (46−63%) during the late Katian was roughly four to nine times larger compared with today, which corresponds to at least 5% (potentially tens of percent) of the total seafloor area (cf. Wang et al., 2016). The extent of global ocean anoxia at this time overlaps with U isotope model estimates for the OAE2 and late Permian oceans, but was significantly higher than the late Ediacaran (ca. 560–551 Ma) and the modern ocean. Although the highest $\delta^{98}Mo$ in the Fjäcka Shale is about +1.3 ‰, Mo isotope fractionation between seawater and sediments most likely occurred due to incomplete formation of and/or removal of highly particle-reactive Mo sulfide species from bottom waters. Non-quantitative removal of Mo from bottom waters is implied by the high Mo enrichments associated with the highest $\delta^{98}Mo$. The inferred seawater $\delta^{98}Mo$ (+1.4−2.1 ‰) during the late Katian suggests that 10−70% of the riverine Mo flux was removed into the euxinic sink, which probably corresponds to < 1% of the total seafloor

area (the areal extent remains low because Mo removal into euxinic sediments is highly efficient compared to other redox settings), consistent with the pronounced Mo enrichments in the Fjäcka Shale (cf. Dahl et al., 2011; Reinhard et al., 2013; Chen et al., 2015). Therefore, the U and Mo isotope compositions of the Fjäcka Shale demonstrate expanded ocean anoxia and euxinia before the Hirnantian glaciation, respectively. The difference in the extent of seafloor area covered by anoxic waters (euxinic plus ferruginous, at least 5% inferred from U isotopes) and euxinic waters (< 1% inferred from Mo isotopes) highlights that a large aerial extent of ferruginous seafloor existed in the late Katian.

The heaviest δ^{98}Mo in the early Hirnantian (+2.4 ‰) is associated with pronounced Mo enrichments and is similar to modern seawater (+2.3 ‰) (Zhou et al., 2012, 2015), thus suggesting early Hirnantian ocean oxygenation was at a scale similar to that of the modern ocean. Hence, we infer that ocean oxygenation intensified from the late Katian to the early-mid Hirnantian. This interpretation is supported by other geological and geochemical evidence across the Ordovician-Silurian transition (LaPorte et al., 2009; Melchin et al., 2013), suggesting that the first phase of the Hirnantian extinction may be related to rapid global cooling (Brenchley et al., 2001; Melchin et al., 2013) rather than expansion of sulfidic water masses (Zhang et al., 2009; Hammarlund et al., 2012). Our study highlights the advantage of integrating U and Mo isotope data from ORMs to infer the global extent of ferruginous and euxinic conditions in ancient oceans.

Acknowledgements

This study was supported by a NSERC Discovery grant to BK. SMA Mineral generously allowed access to quarries in the Siljan region. AB Igrene permitted sampling of the three Siljan area drill cores used in this study. Collection and documentation of the drill core samples was supported through a grant from ENI S.p.A. to HS and JH. CL acknowledges support from Chinese 973 program (grant No. 2013CB955704) and NSFC (grant No. 41172030). We are grateful to Thomas Algeo, Noah Planavsky, and an anonymous reviewer for their constructive reviews and Michael E. Böttcher for editorial handling.

REFERENCES

Ahmed, M., Lehnert, O., Fuentes, D. and Meinhold, G. (2014) Origin of oil and bitumen in the Late Devonian Siljan impact structure, central Sweden. *Organic Geochemistry, 68*, 13-26. doi: 10.1016/j.orggeochem.2013.12.010

Ainsaar, L., Kaljo, D., Martma, T., Meidla, T., Männik, P., Nõlvak, J. and Tinn, O. (2010) Middle and Upper Ordovician carbon isotope chemostratigraphy in Baltoscandia: A correlation standard and clues to environmental history. *Palaeogeography, Palaeoclimatology, Palaeoecology, 294*(3-4), 189-201. doi: 0.1016/j.palaeo.2010.01.003

Algeo, T. J. and Lyons, T. W. (2006) Mo-total organic carbon covariation in modern anoxic marine environments: Implications for analysis of paleoredox and paleohydrographic conditions. *Paleoceanography, 21*, PA1016. doi: 10.1029/2004pa001112

Algeo, T. J. and Maynard, J. B. (2004) Trace-element behavior and redox facies in core shales of Upper Pennsylvanian Kansas-type cyclothems. *Chemical Geology, 206*(3-4), 289-318. doi: 10.1016/j.chemgeo.2003.12.009

Algeo, T. J. and Tribovillard, N. (2009) Environmental analysis of paleoceanographic systems based on molybdenum–uranium covariation. *Chemical Geology, 268*(3-4), 211-225. doi: 10.1016/j.chemgeo.2009.09.001

Anbar, A. D., Duan, Y., Lyons, T. W., Arnold, G. L., Kendall, B., Creaser, R. A., Kaufman, A. J., Gordon, G. W., Scott, C., Garvin, J. and Buick, R. (2007) A Whiff of Oxygen Before the Great Oxidation Event? *Science, 317*(5846), 1903-1906. doi: 10.1126/science.1140325

Andersen, M. B., Romaniello, S., Vance, D., Little, S. H., Herdman, R. and Lyons, T. W. (2014) A modern framework for the interpretation of $^{238}U/^{235}U$ in studies of ancient ocean redox. *Earth and Planetary Science Letters, 400*, 184-194. doi: 10.1016/j.epsl.2014.05.051

Andersen, M. B., Elliott, T., Freymuth, H., Sims, K. W., Niu, Y. and Kelley, K. A. (2015) The terrestrial uranium isotope cycle. *Nature, 517*(7534), 356-359. doi: 10.1038/nature14062

Andersen, M. B., Vance, D., Morford, J. L., Bura-Nakić, E., Breitenbach, S. F. M. and Och, L. (2016) Closing in on the marine $^{238}U/^{235}U$ budget. *Chemical Geology, 420*, 11-22. doi: 10.1016/j.chemgeo.2015.10.041

Anderson, R. F. (1987) Redox behavior of uranium in an anoxic marine basin. *Uranium, 3*(2-4), 145-164.

Anderson, R. F., Fleisher, M. Q. and Lehuray, A. P. (1989) Concentration, oxidation state, and particulate flux of uranium in the Black Sea. *Geochimica et Cosmochimica Acta, 53*, 2215-2224.

Anderson, T. F. and Raiswell, R. (2004) Sources and mechanisms for the enrichment of highly reactive iron in euxinic Black Sea sediments. *American Journal of Science, 304*, 203-233.

Archer, C. and Vance, D. (2008) The isotopic signature of the global riverine molybdenum flux and anoxia in the ancient oceans. *Nature Geoscience, 1*(9), 597-600. doi: 10.1038/ngeo282.

Ardakani, O. H., Chappaz, A., Sanei, H. and Mayer B. (2016) Effects of thermal maturity on remobilization of molybdenum in black shales. *Earth and Planetary Science Letters, 449*, 311-320.

Arnold, G. L., Anbar, A. D., Barling, J. and Lyons, T. W. (2004) Molybdenum isotope evidence for widespread anoxia in mid-Proterozoic oceans. *Science, 304*(5667), 87-90. doi: 10.1126/science.1091785

Asael, D., Tissot, F. L. H., Reinhard, C. T., Rouxel, O., Dauphas, N., Lyons, T. W., Ponzevera, E., Liorzou, C. and Chéron, S. (2013) Coupled molybdenum, iron and uranium stable isotopes as oceanic paleoredox proxies during the Paleoproterozoic Shunga Event. *Chemical Geology, 362*, 193-210. doi: 10.1016/j.chemgeo.2013.08.003

Barling, J., Arnold, G. L. and Anbar, A. D. (2001) Natural mass-dependent variations in the isotopic composition of molybdenum. *Earth and Planetary Science Letters, 193*, 447-457.

Barnes, C. E. and Cochran, J. K. (1990) Uranium removal in oceanic sediments and the oceanic U balance. *Earth and Planetary Science Letters, 97,* 94-101.

Basu, A., Sanford, R. A., Johnson, T. M., Lundstrom, C. C. and Löffler, F. E. (2014) Uranium isotopic fractionation factors during U(VI) reduction by bacterial isolates. *Geochimica et Cosmochimica Acta, 136,* 100-113. doi: 10.1016/j.gca.2014.02.041

Bauert, H., Isozaki, Y., Holmer, L. E., Aoki, K., Sakata, S. and Hirata, T. (2014) New U–Pb zircon ages of the Sandbian (Upper Ordovician) "Big K-bentonite" in Baltoscandia (Estonia and Sweden) by LA-ICPMS. *GFF, 136*(1), 30-33. doi: 10.1080/11035897.2013.862854

Bergström, S. M., Chen, X. U., Gutiérrez-Marco, J. C. and Dronov, A. (2009) The new chronostratigraphic classification of the Ordovician System and its relations to major regional series and stages and to $\delta^{13}C$ chemostratigraphy. *Lethaia, 42*(1), 97-107. doi: 10.1111/j.1502-3931.2008.00136.x

Bergström, S. M., Huff, W. D., Saltzman, M. R., Kolata, D. R. and Leslie, S. A. (2004) The greatest volcanic ash falls in the Phanerozoic: Trans-Atlantic relations of the Ordovician Millbrig and Kinnekulle K-Bentonites. *The Sedimentary Record, 2*(4), 4-8.

Bergström, S. M., Saltzman, M. M. and Schmitz, B. (2006) First record of the Hirnantian (Upper Ordovician) $\delta^{13}C$ excursion in the North American Midcontinent and its regional implications. *Geological Magazine, 143*(05), 657-678. doi: 10.1017/s0016756806002469

Bergström, S. M., Toprak, F. Ö., Huff, W. D. and Mundil, R. (2008) Implications of a new, biostratigraphically well-controlled, radio-isotopic age for the lower Telychian Stage of the Llandovery Series (Lower Silurian, Sweden). *Episodes, 31*, 309-314.

Bergström, S. M., Young, S. and Schmitz, B. (2010) Katian (Upper Ordovician) $\delta^{13}C$ chemostratigraphy and sequence stratigraphy in the United States and Baltoscandia: A regional comparison. *Palaeogeography, Palaeoclimatology, Palaeoecology, 296*(3-4), 217-234. doi: 10.1016/j.palaeo.2010.02.035

Biegeleisen, J. (1996) Nuclear Size and Shape Effects in Chemical Reactions. Isotope Chemistry of the Heavy Elements. *Journal of the American Chemical Society, 118*, 3676-3680.

Brenchley, P.J. (1989) The Late Ordovician extinction, *in* Donovan, S.K., ed., Mass Extinctions: Processes and Evidence: London, Belhaven Press, p. 104–132.

Brenchley, P. J., Carden, G. A., Hints, L., Kaljo, D., Marshall, J. D., Martma, T., Meidla, T. and Nõlvak, J. (2003) High-resolution stable isotope stratigraphy of Upper Ordovician sequences: Constraints on the timing of bioevents and environmental changes associated with mass extinction and glaciation. *Geological Society of America Bulletin, 115*, 89-104.

Brenchley, P. J., Marshall, J. D., Carden, G. A. F., Robertson, D. B. R., Long, D. G. F., Meidla, T., Hints, L. and Anderson, T. F. (1994) Bathymetric and isotopic evidence for a short-lived Late Ordovician glaciation in a greenhouse period. *Geology, 22*, 295-298.

Brenchley, P. J., Marshall, J. D. and Underwood, C. J. (2001) Do all mass extinctions represent an ecological crisis? Evidence from the Late Ordovician. *Geological Journal, 36,* 329-340.

Brennecka, G. A., Herrmann, A. D., Algeo, T. J. and Anbar, A. D. (2011a) Rapid expansion of oceanic anoxia immediately before the end-Permian mass extinction. *Proceedings of the National Academy of Sciences, 108,* 17631-17634. doi: 10.1073/pnas.1106039108/-/DCSupplemental

Brennecka, G. A., Wasylenki, L. E., Bargar, J. R., Weyer, S. and Anbar, A. D. (2011b) Uranium isotope fractionation during adsorption to Mn-oxyhydroxides. *Environmental Science and Technology, 45*(4), 1370-1375. doi: 10.1021/es103061v

Canfield, D. E., Poulton, S. W., Knoll, A. H., Narbonne, G. M., Ross, G., Goldberg, T. and Strauss, H. (2008) Ferruginous conditions dominated later neoproterozoic deep-water chemistry. *Science, 321*(5891), 949-952. doi: 10.1126/science.1154499

Canfield, D. E., Raiswell, R., Westrich, J. T., Reaves, C. M. and Berner, R. A. (1986) The use of chromium reduction in the analysis of reduced inorganic sulfur in sediments and shales. *Chemical Geology, 54,* 149-155.

Cederbom, C., Larson, S. A., Tullborg, E. and Stiberg, J. (2000) Fission track thermochronology applied to Phanerozoic thermotectonic events in central and southern Sweden. *Tectonophysics, 316,* 153-167.

Chappaz, A., Lyons, T. W., Gregory, D. D., Reinhard, C. T., Gill, B. C., Li, C. and Large, R. R. (2014) Does pyrite act as an important host for molybdenum in modern and ancient euxinic sediments? *Geochimica et Cosmochimica Acta, 126,* 112-122. doi: 10.1016/j.gca.2013.10.028

Chen, X., Ling, H. F., Vance, D., Shields-Zhou, G. A., Zhu, M., Poulton, S. W., Och, L. M., Jiang, S. Y., Li, D., Cremonese, L. and Archer, C. (2015) Rise to modern levels of ocean oxygenation coincided with the Cambrian radiation of animals. *Nature Communications, 6*, 7142. doi: 10.1038/ncomms8142

Chen, X., Romaniello, S. J., Herrmann, A. D., Wasylenki, L. E., Anbar, A. D. (2016) Uranium isotope fractionation during coprecipitation with aragonite and calcite. *Geochimica et Cosmochimica Acta,188*, 189-207.

Cheng, M., Li, C., Zhou, L. and Xie, S. C. (2015) Mo marine geochemistry and reconstruction of ancient ocean redox states. *Science China Earth Science*, *58*, 2123–2133.

Cheng, M., Li, C., Zhou, L., Algeo, T. J., Zhang, F-F., Romaniello, S., Jin, C-S., Lei, L-D., Feng, L-J. and Jiang, S-Y. (2016) Marine Mo biogeochemistry in the context of dynamically euxinic mid-depth waters: A case study of the lower Cambrian Niutitang shales, South China. *Geochimica et Cosmochimica Acta*, 183, 79-93. Doi: 10.1016/j.gca.2016.03.035

Cherns, L. and Wheeley, J. R. (2007) A pre-Hirnantian (Late Ordovician) interval of global cooling – The Boda event re-assessed. *Palaeogeography, Palaeoclimatology, Palaeoecology, 251*(3-4), 449-460. doi: 10.1016/j.palaeo.2007.04.010

Christidis, G. E. and Huff, W. D. (2009) Geological Aspects and Genesis of Bentonites. *Elements, 5*(2), 93-98. doi: 10.2113/gselements.5.2.93

Cocks, L. R. M. and Torsvik, T. H. (2002) Earth geography from 500 to 400 million years ago: a faunal and palaeomagnetic review. *Journal of the Geological Society, London, 159*, 631-644.

Cocks, L. R. M. and Torsvik, T. H. (2005) Baltica from the late Precambrian to mid-Palaeozoic times: The gain and loss of a terrane's identity. *Earth-Science Reviews, 72*(1-2), 39-66. doi: 10.1016/j.earscirev.2005.04.001

Cohen, K. M., Finney, S. C., Gibbard, P. L. and Fan, J. (2013) The ICS International Chronostratigraphic Chart. *Episodes, 36*(3), 199-204.

Cramer, B. D., Brett, C. E., Melchin, M. J., Männik, P., Kleffner, M. A., McLaughlin, P. I., Loydell, D. K., Munnecke, A., Jeppsson, L., Corradini, C., Brunton, F. R. and Saltzman, M. R. (2011) Revised correlation of Silurian Provincial Series of North America with global and regional chronostratigraphic units and $\delta^{13}C_{carb}$ chemostratigraphy. *Lethaia, 44*(2), 185-202. doi: 10.1111/j.1502-3931.2010.00234.x

Crusius, J., Calvert, S., Pedersen, T. and Sage, D. (1996) Rhenium and molybdenum enrichments in sediments as indicators of oxic, suboxic and sulfidic conditions of deposition. *Earth and Planetary Science Letters, 145*, 65-78.

Dahl, T. W., Hammarlund, E. U., Anbar, A. D., Bond, D. P. G., Gill, B. C., Gordon, G. W., Knoll, A. H., Nielsen, A. T., Schovsbo, N. H. and Canfield, D. E. (2010a) Devonian rise in atmospheric oxygen correlated to the radiations of terrestrial plants and large predatory fish. *Proceedings of the National Academy of Sciences, 107*(42), 17911-17915. doi: 10.1073/pnas.1011287107/-/DCSupplemental.

Dahl, T. W., Anbar, A. D., Gordon, G. W., Rosing, M. T., Frei, R. and Canfield, D. E. (2010b) The behavior of molybdenum and its isotopes across the chemocline and in the sediments of sulfidic Lake Cadagno, Switzerland. *Geochimica et Cosmochimica Acta, 74*(1), 144-163. doi: 10.1016/j.gca.2009.09.018

Dahl, T. W., Canfield, D. E., Rosing, M. T., Frei, R. E., Gordon, G. W., Knoll, A. H. and Anbar, A. D. (2011) Molybdenum evidence for expansive sulfidic water masses in ~750Ma oceans. *Earth and Planetary Science Letters, 311*(3-4), 264-274. doi: 10.1016/j.epsl.2011.09.016

Dahl, T. W., Chappaz, A., Fitts, J. P. and Lyons, T. W. (2013) Molybdenum reduction in a sulfidic lake: Evidence from X-ray absorption fine-structure spectroscopy and implications for the Mo paleoproxy. *Geochimica et Cosmochimica Acta, 103*, 213-231. doi: 10.1016/j.gca.2012.10.058

Delabroye, A., and Vecoli, M. (2010) The end-Ordovician glaciation and the Hirnantian Stage: A global review and questions about Late Ordovician event stratigraphy. *Earth-Science Reviews, 98*(3-4), 269-282. doi: 10.1016/j.earscirev.2009.10.010

Dhuime, B., Wuestefeld, A. and Hawkesworth C. J. (2015) Emergence of modern continental crust about 3 billion years ago. *Nature Geoscience, 8*, 552-555.

Dickson, A. J. and Cohen, A. S. (2012) A molybdenum isotope record of Eocene Thermal Maximum 2: Implications for global ocean redox during the early Eocene. *Paleoceanography, 27*(3), PA3230. doi: 10.1029/2012pa002346

Dickson, A. J., Cohen, A. S. and Coe, A. L. (2012) Seawater oxygenation during the Paleocene-Eocene Thermal Maximum. *Geology, 40*(7), 639-642. doi: 10.1130/g32977.1

Duan, Y., Anbar, A. D., Arnold, G. L., Lyons, T. W., Gordon, G. W. and Kendall, B. (2010) Molybdenum isotope evidence for mild environmental oxygenation before the Great Oxidation Event. *Geochimica et Cosmochimica Acta, 74*(23), 6655-6668. doi: 10.1016/j.gca.2010.08.035

Dunk, R. M., Mills, R. A. and Jenkins, W. J. (2002) A reevaluation of the oceanic uranium budget for the Holocene. *Chemical Geology, 190*, 45-67.

Ebbestad, J. O. R. and Högström, A. E. S. (2007) Ordovician of the Siljan district, Sweden. In: Ebbestad, J. O. R., Wickström, L. M., Högström, A. E. S. (Eds.) WOGOGOB 2007. 9th Meeting of the Working Group on Ordovician Geology of Baltoscandia. Field guide and Abstracts. *Sveriges Geologiska Undersökning Rapporter och meddelanden, 128*, 7-26.

Ebbestad, J. O. R., Högström, A. E. S., Frisk, Å. M., Martma, T., Kaljo, D., Kröger, B. and Pärnaste, H. (2014) Terminal Ordovician stratigraphy of the Siljan district, Sweden. *GFF*, 1-21. doi: 10.1080/11035897.2014.945620

Emerson, S. R. and Huested, S. S. (1991) Ocean anoxia and the concentrations of molybdenum and vanadium in seawater. *Marine Chemistry, 34*, 177-196.

Erickson, B. E. and Helz, G. R. (2000) Molybdenum(VI) speciation in sulfidic waters: Stability and lability of thiomolybdates. *Geochimica et Cosmochimica Acta, 64*(7), 1149-1158.

Finnegan, S., Bergmann, K., Eiler, J. M., Jones, D. S., Fike, D. A., Eisenman, I., Hughes, N. C., Tripati, A. K. and Fischer, W. W. (2011) The Magnitude and Duration of Late Ordovician - Early Silurian Glaciation. *Science, 331*, 903-906.

Finney, S. C., Berry, W. B. N., Cooper, J. D., Ripperdan, R. L., Sweet, W. C., Jacobson, S. R., Soufiane, A., Achab, A. and Noble, P. J. (1999) Late Ordovician mass extinction: A new perspective from stratigraphic sections in central Nevada. *Geology, 27*, 215-218.

Fortey, R. A. and Cocks, L. R. M. (2005) Late Ordovician global warming—The Boda event. *Geology, 33*(5), 405-408. doi: 10.1130/g21180.1

Georgiev, S., Stein, H.J., Hannah, J.L., Bingen, B., Weiss, H.M., and Piasecki, S. (2011) Hot acidic Late Permian seas stifle life in record time: *Earth and Planetary Science Letters*, v. 310, p. 389-400.

Goldberg, T., Archer, C., Vance, D. and Poulton, S. W. (2009) Mo isotope fractionation during adsorption to Fe (oxyhydr)oxides. *Geochimica et Cosmochimica Acta, 73*(21), 6502-6516. doi:10.1016/j.gca.2009.08.004

Goldberg, T., Archer, C., Vance, D., Thamdrup, B., McAnena, A. and Poulton, S. W. (2012) Controls on Mo isotope fractionations in a Mn-rich anoxic marine sediment, Gullmar Fjord, Sweden. *Chemical Geology, 296-297*, 73-82. doi: 10.1016/j.chemgeo.2011.12.020

Goldberg, T., Gordon, G., Izon, G., Archer, C., Pearce, C. R., McManus, J., Anbar, A. D. and Rehkämper, M. (2013) Resolution of inter-laboratory discrepancies in Mo isotope data: an intercalibration. *Journal of Analytical Atomic Spectrometry, 28*(5), 724. doi: 10.1039/c3ja30375f

Gordon, G. W., Lyons, T. W., Arnold, G. L., Roe, J., Sageman, B. B. and Anbar, A. D. (2009) When do black shales tell molybdenum isotope tales? *Geology, 37*(6), 535-538. doi: 10.1130/g25186a.1

Gorjan, P., Kaiho, K., Fike, D. A. and Xu, C. (2012) Carbon- and sulfur-isotope geochemistry of the Hirnantian (Late Ordovician) Wangjiawan (Riverside) section, South China: Global correlation and environmental event interpretation.

Palaeogeography, Palaeoclimatology, Palaeoecology, 337-338, 14-22. doi: 10.1016/j.palaeo.2012.03.021

Goto, K. T., Anbar, A. D., Gordon, G. W., Romaniello, S. J., Shimoda, G., Takaya, Y., Tokumaru, A., Nozaki, T., Suzuki, K., Machida, S., Hanyu, T. and Usui, A. (2014) Uranium isotope systematics of ferromanganese crusts in the Pacific Ocean: Implications for the marine $^{238}U/^{235}U$ isotope system. *Geochimica et Cosmochimica Acta, 146*, 43-58. doi: 10.1016/j.gca.2014.10.003

Grahn, Y. (1998) Lower Silurian (Llandovery-Middle Wenlock) Chitinozoa and biostratigraphy of the mainland of Sweden. *GFF, 120*(3), 273-283. doi: 10.1080/11035899809453218

Grieve, R. A. F. (1988) The formation of large impact structures and constraints on the nature of Siljan. In A. Boden & K. G. Eriksson (eds.): Deep drilling in crystalline bedrock, 328-348. Vol. 1. The deep gas drilling in the Siljan impact structure, Sweden and Astroblemes Proceeding of the International Symposium. Springer Verlag, Berlin

Hammarlund, E. U., Dahl, T. W., Harper, D. A. T., Bond, D. P. G., Nielsen, A. T., Bjerrum, C. J., Schovsbo, N. H., Schönlaub, H. P., Zalasiewicz, J. A. and Canfield, D. E. (2012) A sulfidic driver for the end-Ordovician mass extinction. *Earth and Planetary Science Letters, 331-332*, 128-139. doi: 10.1016/j.epsl.2012.02.024

Haq, B. U. and Schutter, S. R. (2008) A Chronology of Paleozoic Sea-Level Changes. *Science, 322*, 64-68.

Helz, G. R., Bura-Nakić, E., Mikac, N. and Ciglenečki, I. (2011) New model for molybdenum behavior in euxinic waters. *Chemical Geology, 284*(3-4), 323-332. doi: 10.1016/j.chemgeo.2011.03.012

Helz, G. R., Miller, C. V., Charnock, J. M., Mosselmans, J. F. W., Pattrick, R. A. D., Garner, C. D. and Vaughan, D. J. (1996) Mechanism of molybdenum removal from the sea and its concentration in black shales: EXAFS evidence. *Geochimica et Cosmochimica Acta, 60*(19), 3631-3642.

Herrmann, A. D., Haupt, B. J., Patzkowsky, M. E., Seidov, D. and Slingerland, R. L. (2004) Response of Late Ordovician paleoceanography to changes in sea level, continental drift, and atmospheric pCO_2: potential causes for long-term cooling and glaciation. *Palaeogeography, Palaeoclimatology, Palaeoecology, 210*(2-4), 385-401. doi:10.1016/j.palaeo.2004.02.034

Herrmann, A. D., Kendall, B., Algeo, T. J., Gordon, G. W., Wasylenki, L. E. and Anbar, A. D. (2012) Anomalous molybdenum isotope trends in Upper Pennsylvanian euxinic facies: Significance for use of δ^{98}Mo as a global marine redox proxy. *Chemical Geology, 324-325*, 87-98. doi: 10.1016/j.chemgeo.2012.05.013

Högström, A. E. S., Sturkell, E., Ebbestad, J. O. R., Lindström, M. and Ormö, J. (2010) Concentric impact structures in the Palaeozoic of Sweden – the Lockne and Siljan craters. *GFF, 132*(1), 65-70. doi: 10.1080/11035890903469971

Holm, S., Alwmark, C., Alvarez, W. and Schmitz, B. (2011) Shock barometry of the Siljan impact structure, Sweden. *Meteoritics and Planetary Science, 46*(12), 1888-1909. doi: 10.1111/j.1945-5100.2011.01303.x

Holmden, C., Amini, M. and Francois, R. (2015) Uranium isotope fractionation in Saanich Inlet: A modern analog study of a paleoredox tracer. *Geochimica et Cosmochimica Acta, 153*, 202-215. doi: 10.1016/j.gca.2014.11.012

Huff, W. D., Kolata, D. R., Bergström, S. M. and Zhang, Y. (1996) Large-magnitude Middle Ordovician volcanic ash falls in North America and Europe: dimensions, emplacement and post-emplacement characteristics. *Journal of Volcanology and Geothermal Research, 73*, 285-301.

Huigen, Y. and Andriessen, P. (2004) Thermal effects of Caledonian foreland basin formation, based on fission track analyses applied on basement rocks in central Sweden. *Physics and Chemistry of the Earth, Parts A/B/C, 29*(10), 683-694. doi: 10.1016/j.pce.2004.03.006

Jones, D. S., & Fike, D. A. (2013). Dynamic sulfur and carbon cycling through the end-Ordovician extinction revealed by paired sulfate–pyrite $\delta^{34}S$. *Earth and Planetary Science Letters, 363*, 144-155. doi:10.1016/j.epsl.2012.12.015

Jourdan, F., Reimold, W. U. and Deutsch, A. (2012) Dating Terrestrial Impact Structures. *Elements, 8*(1), 49-53. doi: 10.2113/gselements.8.1.49

Juhlin, C., Sturkell, E., Ebbestad, J. O. R., Lehnert, O., Högström, A. E. S. and Meinhold, G. (2012) A new interpretation of the sedimentary cover in the western Siljan Ring area, central Sweden, based on seismic data. *Tectonophysics, 580*, 88-99. doi: 10.1016/j.tecto.2012.08.040

Kendall, B., Brennecka, G. A., Weyer, S. and Anbar, A. D. (2013) Uranium isotope fractionation suggests oxidative uranium mobilization at 2.50Ga. *Chemical Geology, 362*, 105-114. doi: 10.1016/j.chemgeo.2013.08.010

Kendall, B., Creaser, R. A., Gordon, G. W. and Anbar, A. D. (2009) Re–Os and Mo isotope systematics of black shales from the Middle Proterozoic Velkerri and Wollogorang Formations, McArthur Basin, northern Australia. *Geochimica et Cosmochimica Acta, 73*(9), 2534-2558. doi: 10.1016/j.gca.2009.02.013

Kendall, B., Gordon, G. W., Poulton, S. W. and Anbar, A. D. (2011) Molybdenum isotope constraints on the extent of late Paleoproterozoic ocean euxinia. *Earth and Planetary Science Letters, 307*(3-4), 450-460. doi: 10.1016/j.epsl.2011.05.019

Kendall, B., Komiya, T., Lyons, T. W., Bates, S. M., Gordon, G. W., Romaniello, S. J., Jiang, G., Creaser, R. A., Xiao, S., McFadden, K., Sawaki, Y., Tahata, M., Shu, D., Han, J., Li, Y., Chu, X. and Anbar, A. D. (2015) Uranium and molybdenum isotope evidence for an episode of widespread ocean oxygenation during the late Ediacaran Period. *Geochimica et Cosmochimica Acta, 156*, 173-193. doi: 10.1016/j.gca.2015.02.025

Kendall, B., Reinhard, C. T., Lyons, T. W., Kaufman, A. J., Poulton, S. W. and Anbar, A. D. (2010) Pervasive oxygenation along late Archaean ocean margins. *Nature Geoscience, 3*, 647-652. doi: 10.1038/ngeo942

Komor, S. C., Valley, J. W. and Brown, P. E. (1988) Fluid-inclusion evidence for impact heating at the Siljan Ring, Sweden. *Geology, 16*, 711-715.

Kröger, B., Ebbestad, J. O. R. and Lehnert, O. (2016) Accretionary mechanisms and temporal sequence of Formation of the Boda Limestone mud-mounds (Upper Ordovician), Siljan district, Sweden. *Journal of Sedimentary Research, 86*, 363-379

Ku, T. L., Knauss, K. G. and Mathieu, G. G. (1977) Uranium in open ocean: concentration and isotopic composition*. *Deep Sea Research, 24*, 1005-1017.

Kump, L. R., Arthur, M. A., Patzkowsky, M. E., Gibbs, M. T., Pinkus, D. S. and Sheehan, P. M. (1999) A weathering hypothesis for glaciation at high atmospheric pCO2 during the Late Ordovician. *Palaeogeography, Palaeoclimatology, Palaeoecology, 152*, 173-187.

Kurzweil, F., Wille, M., Schoenberg, R., Taubald, H. and Van Kranendonk, M. J. (2015) Continuously increasing δ^{98}Mo values in Neoarchean black shales and iron formations from the Hamersley Basin. *Geochimica et Cosmochimica Acta, 164*, 523-542. doi: 10.1016/j.gca.2015.05.009

Langmuir, D. (1978) Uranium solution-mineral equilibria at low temperatures with applications to sedimentary ore deposits. *Geochimica et Cosmochimica Acta, 42*, 547-569.

LaPorte, D. F., Holmden, C., Patterson, W. P., Loxton, J. D., Melchin, M. J., Mitchell, C. E., Finney, S. C. and Sheets, H. D. (2009) Local and global perspectives on carbon and nitrogen cycling during the Hirnantian glaciation. *Palaeogeography, Palaeoclimatology, Palaeoecology, 276*(1-4), 182-195. doi: 10.1016/j.palaeo.2009.03.009

Larson, S. A., Tullborg, E., Cederbom, C. and Stiberg, J. (1999) Sveconorwegian and Caledonian foreland basins in the Baltic Shield revealed by fission-track thermochronology. *Terra Nova, 11*, 210-215.

Lehnert, O., Meinhold, G., Arslan, A., Ebbestad, J. O. R. and Calner, M. (2013) Ordovician stratigraphy of the Stumsnäs 1 drill core from the southern part of the Siljan Ring, central Sweden. *GFF, 135*(2), 204-212. doi: 10.1080/11035897.2013.813582

Lehnert, O., Meinhold, G., Bergström, S. M., Calner, M., Ebbestad, J. O. R., Egenhoff, S., Frisk, Å. M., Hannah, J. L., Högström, A. E. S., Huff, W. D., Juhlin, C., Maletz, J., Stein, H. J., Sturkell, E. and Vandenbroucke, T. R. A. (2012) New Ordovician–Silurian drill cores from the Siljan impact structure in central Sweden: an integral part of the Swedish Deep Drilling Program. *GFF*, *134*(2), 87-98. doi: 10.1080/11035897.2012.692707

Li, C., Love, G. D., Lyons, T. W., Fike, D. A., Sessions, A. L. and Chu, X. (2010) A stratified redox model for the Ediacaran ocean. *Science*, *328*(5974), 80-83. doi: 10.1126/science.1182369

Li, C., Planavsky, N. J., Shi, W. Zhang, Z-H., Zhou, C-M., Cheng, M., Tarhan, L. G., Luo, G-M., and Xie, S-C. (2015) Ediacaran Marine Redox Heterogeneity and Early Animal Ecosystems. *Scientific Reports*, *2015*, 5, 17097.

Lorenz, H. (2010) The Swedish Deep Drilling Program: For Science and Society. *GFF*, *132*(1), 25-27. doi: 10.1080/11035891003763354

Lyons, T. W. and Severmann, S. (2006) A critical look at iron paleoredox proxies: New insights from modern euxinic marine basins. *Geochimica et Cosmochimica Acta*, *70*(23), 5698-5722. doi: 10.1016/j.gca.2006.08.021

Marshall, J. D. and Middleton, P. D. (1990) Changes in marine isotopic composition and the Late Ordovician glaciation. *Journal of the Geological Society, London*, *147*, 1-4.

März, C., Poulton, S. W., Beckmann, B., Küster, K., Wagner, T. and Kasten, S. (2008) Redox sensitivity of P cycling during marine black shale formation: Dynamics of sulfidic and anoxic, non-sulfidic bottom waters. *Geochimica et Cosmochimica Acta*, *72*(15), 3703-3717. doi: 10.1016/j.gca.2008.04.025

McLennan, S. M. (2001) Relationships between the trace element composition of sedimentary rocks and upper continental crust. *Geochemistry, Geophysics, Geosystems, 2*, Paper number 2000GC000109.

McManus, J., Berelson, W. M., Severmann, S., Poulson, R. L., Hammond, D. E., Klinkhammer, G. P. and Holm, C. (2006) Molybdenum and uranium geochemistry in continental margin sediments: Paleoproxy potential. *Geochimica et Cosmochimica Acta, 70*(18), 4643-4662. doi: 10.1016/j.gca.2006.06.1564

Melchin, M. J. and Holmden, C. (2006) Carbon isotope chemostratigraphy in Arctic Canada: Sea-level forcing of carbonate platform weathering and implications for Hirnantian global correlation. *Palaeogeography, Palaeoclimatology, Palaeoecology, 234*(2-4), 186-200. doi: 10.1016/j.palaeo.2005.10.009

Melchin, M. J., Mitchell, C. E., Holmden, C. and Storch, P. (2013) Environmental changes in the Late Ordovician-Early Silurian: Review and new insights from black shales and nitrogen isotopes. *Geological Society of America Bulletin, 125*(11-12), 1635-1670. doi: 10.1130/b30812.1

Miller, C. A., Peucker-Ehrenbrink, B., Walker, B. D. and Marcantonio, F. (2011) Re-assessing the surface cycling of molybdenum and rhenium. *Geochimica et Cosmochimica Acta, 75*(22), 7146-7179. doi: 10.1016/j.gca.2011.09.005

Montoya-Pino, C., Weyer, S., Anbar, A. D., Pross, J., Oschmann, W., van de Schootbrugge, B. and Arz, H. W. (2010) Global enhancement of ocean anoxia during Oceanic Anoxic Event 2: A quantitative approach using U isotopes. *Geology, 38*(4), 315-318. doi: 10.1130/g30652.1

Morford, J. L. and Emerson, S. (1999) The geochemistry of redox sensitive trace metals in sediments. *Geochimica et Cosmochimica Acta, 63*(11/12), 1735-1750.

Morford, J. L., Emerson, S. R., Breckel, E. J. and Kim, S. H. (2005) Diagenesis of oxyanions (V, U, Re, and Mo) in pore waters and sediments from a continental margin. *Geochimica et Cosmochimica Acta*, *69*(21), 5021-5032. doi: 10.1016/j.gca.2005.05.015

Nägler, T. F., Siebert, C., Lüschen, H. and Böttcher, M. E. (2005) Sedimentary Mo isotope record across the Holocene fresh–brackish water transition of the Black Sea. *Chemical Geology*, *219*(1-4), 283-295. doi: 10.1016/j.chemgeo.2005.03.006

Nägler, T. F., Neubert, N., Böttcher, M. E., Dellwig, O. and Schnetger, B. (2011) Molybdenum isotope fractionation in pelagic euxinia: Evidence from the modern Black and Baltic Seas. *Chemical Geology*, *289*(1-2), 1-11. doi: 10.1016/j.chemgeo.2011.07.001

Nägler, T. F., Anbar, A. D., Archer, C., Goldberg, T., Gordon, G. W., Greber, N. D., Siebert, C., Sohrin, Y. and Vance, D. (2014) Proposal for an International Molybdenum Isotope Measurement Standard and Data Representation. *Geostandards and Geoanalytical Research*, *38*(2), 149-151. doi: 10.1111/j.1751-908X.2013.00275.x

Nakagawa, Y., Takano, S., Firdaus, M. L., Norsuye, K., Hirata, T., Vance, D. and Sohrin, Y. (2012) The molybdenum isotopic composition of the modern ocean. *Geochimica et Cosmochimica Acta, 46*, 131-141.

Neubert, N., Nägler, T. F. and Böttcher, M. E. (2008) Sulfidity controls molybdenum isotope fractionation into euxinic sediments: Evidence from the modern Black Sea. *Geology, 36*(10), 775-778. doi: 10.1130/g24959a.1

Noordmann, J., Weyer, S., Georg, R. B., Jons, S. and Sharma, M. (2016) $^{238}U/^{235}U$ isotope ratios of crustal material, rivers and products of hydrothermal alteration: new insights on the oceanic U isotope mass balance. *Isotopes in Environmental and Health Studies, 52*(1-2), 141-163. doi:10.1080/10256016.2015.1047449

Noordmann, J., Weyer, S., Montoya-Pino, C., Dellwig, O., Neubert, N., Eckert, S., Paetzel, M. and Böttcher, M. E. (2015) Uranium and molybdenum isotope systematics in modern euxinic basins: Case studies from the central Baltic Sea and the Kyllaren fjord (Norway). *Chemical Geology, 396*, 182-195. doi: 10.1016/j.chemgeo.2014.12.012

Nõlvak, J., Hints, O. and Männik, P. (2006) Ordovician timescale in Estonia: recent developments. *Proceedings of the Estonian Academy of Sciences, Geology, 55*, 95-108.

Partin, C. A., Bekker, A., Planavsky, N. J., Scott, C. T., Gill, B. C., Li, C., Podkovyrov, V., Maslov, A., Konhauser, K. O., Lalonde, S. V., Love, G. D., Poulton, S. W. and Lyons, T. W. (2013) Large-scale fluctuations in Precambrian atmospheric and oceanic oxygen levels from the record of U in shales. *Earth and Planetary Science Letters, 369-370*, 284-293. doi: 10.1016/j.epsl.2013.03.031

Partin, C. A., Bekker, A., Planavsky, N. J. and Lyons, T. W. (2015) Euxinic conditions recorded in the ca. 1.93Ga Bravo Lake Formation, Nunavut (Canada): Implications

for oceanic redox evolution. *Chemical Geology, 417*, 148-162. doi: 10.1016/j.chemgeo.2015.09.004

Pearce, C. R., Burton, K. W., von Strandmann, P. A. E. P., James, R. H. and Gíslason, S. R. (2010) Molybdenum isotope behaviour accompanying weathering and riverine transport in a basaltic terrain. *Earth and Planetary Science Letters, 295*(1-2), 104-114. doi: 10.1016/j.epsl.2010.03.032

Pearce, C. R., Cohen, A. S., Coe, A. L. and Burton, K. W. (2008) Molybdenum isotope evidence for global ocean anoxia coupled with perturbations to the carbon cycle during the Early Jurassic. *Geology, 36*(3), 231. doi: 10.1130/g24446a.1

Planavsky, N. J., McGoldrick, P., Scott, C. T., Li, C., Reinhard, C. T., Kelly, A. E., Chu, X., Bekker, A., Love, G. D. and Lyons, T. W. (2011) Widespread iron-rich conditions in the mid-Proterozoic ocean. *Nature, 477*(7365), 448-451. doi:10.1038/nature10327

Pohl, A., Donnadieu, Y., Le Hir, G., Ladant, J., Dumas, C., Alvarez-Solas, J. and Vandenbroucke, T. R. A. (2016) Glacial onset predated Late Ordovician climate cooling. *Paleoceanography, 31*(6), 800-821. doi:10.1002/2016pa002928Poulson, R. L., Siebert, C., McManus, J. and Berelson, W. M. (2006) Authigenic molybdenum isotope signatures in marine sediments. *Geology, 34*(8), 617. doi: 10.1130/g22485.1

Poulson Brucker, R. L., McManus, J., Severmann, S. and Berelson, W. M. (2009) Molybdenum behavior during early diagenesis. *Geochemistry, Geophysics, Geosystems, 10*(6), Q06010. doi: 10.1029/2008GC002180

Poulton, S. W. and Canfield, D. E. (2005) Development of a sequential extraction procedure for iron: implications for iron partitioning in continentally derived

particulates. *Chemical Geology*, *214*(3-4), 209-221. doi: 10.1016/j.chemgeo.2004.09.003

Poulton, S. W. and Canfield, D. E. (2011) Ferruginous Conditions: A Dominant Feature of the Ocean through Earth's History. *Elements, 7*(2), 107-112. doi: 10.2113/gselements.7.2.107

Poulton, S. W., Fralick, P. W. and Canfield, D. E. (2004) The transition to a sulphidic ocean ~1.84 billion years ago. *Nature, 431*, 173-177. doi: 10.1038/nature02863

Poulton, S. W., Fralick, P. W. and Canfield, D. E. (2010) Spatial variability in oceanic redox structure 1.8 billion years ago. *Nature Geoscience, 3*, 486-490. doi: 10.1038/ngeo889

Poulton, S. W. and Raiswell, R. (2002) The low-temperature geochemical cycle of iron: From continental fluxes to marine sediment deposition. *American Journal of Science, 302*, 774-805.

Proemse, B. C., Grasby, S. E., Wieser, M. E., Mayer, B. and Beauchamp, B. (2013) Molybdenum isotopic evidence for oxic marine conditions during the latest Permian extinction. *Geology*, *41*(9), 967-970. doi: 10.1130/g34466.1

Raiswell, R. and Canfield, D. E. (1998) Sources of iron for pyrite formation in marine sediments. *American Journal of Science, 298*, 219-245.

Reimold, W. U., Kelley, S. P., Sherlock, S. C., Henkel, H. and Koeberl, C. (2005) Laser argon dating of melt breccias from the Siljan impact structure, Sweden: Implications for a possible relationship to Late Devonian extinction events. *Meteoritics and Planetary Science*, *40*(4), 591-607.

Reinhard, C. T., Planavsky, N. J., Robbins, L. J., Partin, C. A., Gill, B. C., Lalonde, S. V., Bekker, A., Konhauser, K. O. and Lyons, T. W. (2013) Proterozoic ocean redox and biogeochemical stasis. *Proceedings of the National Academy of Sciences, 110*(14), 5357-5362. doi: 10.1073/pnas.1208622110

Reinhard, C. T., Raiswell, R., Scott, C., Anbar, A. D. and Lyons, T. W. (2009) A late Archean sulfidic sea stimulated by early oxidative weathering of the continents. *Science, 326*, 713-716. doi: 10.1126/science.1176711

Romaniello, S. J., Herrmann, A. D. and Anbar, A. D. (2013) Uranium concentrations and $^{238}U/^{235}U$ isotope ratios in modern carbonates from the Bahamas: Assessing a novel paleoredox proxy. *Chemical Geology, 362*, 305-316. doi: 10.1016/j.chemgeo.2013.10.002

Sahoo, S. K., Planavsky, N. J., Kendall, B., Wang, X., Shi, X., Scott, C., Anbar, A. D., Lyons, T. W. and Jiang, G. (2012) Ocean oxygenation in the wake of the Marinoan glaciation. *Nature, 489*, 546-549. doi: 10.1038/nature11445

Sahoo, S. K., Planavsky, N. J., Jiang, G., Kendall, B., Owens, J. D., Wang, X., Shi, X., Anbar, A. D. and Lyons, T. W. (in press) Oceanic oxygenation events in the anoxic Ediacaran ocean. *Geobiology*. doi: 10.1111/gbi.12182

Schauble, E. A. (2007) Role of nuclear volume in driving equilibrium stable isotope fractionation of mercury, thallium, and other very heavy elements. *Geochimica et Cosmochimica Acta, 71*(9), 2170-2189. doi: 10.1016/j.gca.2007.02.004

Scholz, F., McManus, J. and Sommer, S. (2013) The manganese and iron shuttle in a modern euxinic basin and implications for molybdenum cycling at euxinic ocean margins. *Chemical Geology, 355*, 56-68. doi: 10.1016/j.chemgeo.2013.07.006

Scott, C. and Lyons, T. W. (2012) Contrasting molybdenum cycling and isotopic properties in euxinic versus non-euxinic sediments and sedimentary rocks: Refining the paleoproxies. *Chemical Geology, 324-325*, 19-27. doi: 10.1016/j.chemgeo.2012.05.012

Scott, C., Lyons, T. W., Bekker, A., Shen, Y., Poulton, S. W., Chu, X. and Anbar, A. D. (2008) Tracing the stepwise oxygenation of the Proterozoic ocean. *Nature, 452*(7186), 456-459. doi: 10.1038/nature06811

Selby, D., Creaser, R. A. and Fowler, M. G. (2007) Re–Os elemental and isotopic systematics in crude oils. *Geochimica et Cosmochimica Acta, 71*(2), 378-386. doi: 10.1016/j.gca.2006.09.005

Servais, T., Harper, D. A. T., Munnecke, A., Owen, A. W. and Sheehan, P. M. (2009) Understanding the Great Ordovician Biodiversification Event (GOBE): Influences of paleogeography, paleoclimate, or paleoecology. *GSA Today, 19*(4/5), 4-10. doi:10.1130/gsatg37a.1

Siebert, C., Kramers, J. D., Meisel, Th., Morel, Ph. and Nägler, Th. F. (2005) PGE, Re-Os, and Mo isotope systematics in Archean and early Proterozoic sedimentary systems as proxies for redox conditions of the early Earth. *Geochimica et Cosmochimica Acta, 69*(7), 1787-1801. doi: 10.1016/j.gca.2004.10.006

Siebert, C., McManus, J., Bice, A., Poulson, R. L. and Berelson, W. M. (2006) Molybdenum isotope signatures in continental margin marine sediments. *Earth and Planetary Science Letters, 241*(3-4), 723-733. doi: 10.1016/j.epsl.2005.11.010

Siebert, C., Nägler, T. F., von Blanckenburg, F. and Kramers, J. D. (2003) Molybdenum isotope records as a potential new proxy for paleoceanography. *Earth and Planetary Science Letters, 211*(1-2), 159-171. doi: 10.1016/s0012-821x(03)00189-4

Sheehan, P. M. (2001) The Late Ordovician mass extinction. *Annual Review of Earth and Planetary Sciences, 29*, 331-364.

Shields, G. A., Carden, G. A. F., Veizer, J., Meidla, T., Rong, J. and Li, R. (2003) Sr, C, and O isotope geochemistry of Ordovician brachiopods: a major isotopic event around the Middle-Late Ordovician transition. *Geochimica et Cosmochimica Acta, 67*(11), 2005-2025. doi: 10.1016/s0016-7037(02)01116-x

Sperling, E. A., Wolock, C. J., Morgan, A. S., Gill, B. C., Kunzmann, M., Halverson, G. P., Macdonald, F. A., Knoll, A. H. and Johnston, D. T. (2015) Statistical analysis of iron geochemical data suggests limited late Proterozoic oxygenation. *Nature, 523*(7561), 451-454. doi:10.1038/nature14589

Stein, H. J., Hannah, J. L., Yang, G., Galimberti, R. and Nali, M. (2014) Ordovician Source Rocks and Devonian Oil Expulsion on Bolide Impact at Siljan, Sweden - The Re-Os Story. *Society of Petroleum Engineers - International Petroleum Technology Conference 2014, IPTC 2014 Unlocking Energy Through Innovation, Technology and Capability, 4*, 3212-3217.

Stein, H. J., Hannah, J. L., Zimmerman, A. and Egenhoff, S. (2009) Re-Os fractionation on instantaneous maturation at the Siljan meteorite impact site, central Sweden. *Geochimica et Cosmochimica Acta*, A1268.

Stirling, C. H., Andersen, M. B., Potter, E. and Halliday, A. N. (2007) Low-temperature isotopic fractionation of uranium. *Earth and Planetary Science Letters, 264*(1-2), 208-225. doi: 10.1016/j.epsl.2007.09.019

Stirling, C. H., Andersen, M. B., Warthmann, R. and Halliday, A. N. (2015) Isotope fractionation of ^{238}U and ^{235}U during biologically-mediated uranium reduction. *Geochimica et Cosmochimica Acta, 163*, 200-218. doi: 10.1016/j.gca.2015.03.017

Stylo, M., Neubert, N., Wang, Y., Monga, N., Romaniello, S. J., Weyer, S. and Bernier-Latmani, R. (2015) Uranium isotopes fingerprint biotic reduction. *Proceedings of the National Academy of Sciences, 112*(18), 5619-5624. doi: 10.1073/pnas.1421841112

Svensson, N. B. (1973) Shatter cones from the Siljan struture, central Sweden. *Geologiska Föreningens i Stockholm Förhandlingar, 95*, 139-143.

Tamminen, J. and Wickman, F. E. (1980) Shock effects in pegmatitic quartz from the Siljan ring structure, central Sweden. *Geologiska Föreningens i Stockholm Förhandlingar, 102*, 275-278.

Tang, M., Chen, K. and Rudnick, R. L. (2016) Archean upper crust transition from mafic to felsic marks the onset of plate tectonics. *Science, 351*, 372-375.

Tissot, F. L. H. and Dauphas, N. (2015) Uranium isotopic compositions of the crust and ocean: Age corrections, U budget and global extent of modern anoxia. *Geochimica et Cosmochimica Acta, 167*, 113-143. doi: 10.1016/j.gca.2015.06.034

Tossell, J. A. (2005) Calculating the partitioning of the isotopes of Mo between oxidic and sulfidic species in aqueous solution. *Geochimica et Cosmochimica Acta, 69*(12), 2981-2993. doi:10.1016/j.gca.2005.01.016

Tribovillard, N., Algeo, T. J., Lyons, T. W. and Riboulleau, A. (2006) Trace metals as paleoredox and paleoproductivity proxies: An update. *Chemical Geology, 232*(1-2), 12-32. doi: 10.1016/j.chemgeo.2006.02.012

Tribovillard, N., Riboulleau, A., Lyons, T. and Baudin, F. (2004) Enhanced trapping of molybdenum by sulfurized marine organic matter of marine origin in Mesozoic limestones and shales. *Chemical Geology, 213*(4), 385-401. doi: 10.1016/j.chemgeo.2004.08.011

Trotter, J. A., Williams, I. S., Barnes, C. R., Lécuyer, C. and Nicoll, R. S. (2008) Did Cooling Oceans Trigger Ordovician Biodiversification? Evidence from Conodont Thermometry. *Science, 321*, 550-554.

Vlierboom, F. W., Collini, B. and Zumberge, J. E. (1986) The occurrence of petroleum in sedimentary rocks of the meteor impact crater at Lake Siljan, Sweden. *Organic Geochemistry, 10*, 153-161.

Wang, X., Planavsky, N. J., Reinhard, C. T., Hein, J. R. and Johnson, T. M. (2016) A Cenozoic seawater redox record derived from $^{238}U/^{235}U$ in ferromanganese crusts. *American Journal of Science, 316*(1), 64-83. doi:10.2475/01.2016.02

Webby, B. D., Paris, F., Droser, M. L. and Percival, I. G. (2004) The Great Ordovician Biodiversification Event: Columbia University Press, New York. 484 pp.

Westermann, S., Vance, D., Cameron, V., Archer, C. and Robinson, S. A. (2014) Heterogeneous oxygenation states in the Atlantic and Tethys oceans during Oceanic Anoxic Event 2. *Earth and Planetary Science Letters, 404*, 178-189. doi: 10.1016/j.epsl.2014.07.018

Weyer, S., Anbar, A. D., Gerdes, A., Gordon, G. W., Algeo, T. J. and Boyle, E. A. (2008) Natural fractionation of $^{238}U/^{235}U$. *Geochimica et Cosmochimica Acta, 72*(2), 345-359. doi: 10.1016/j.gca.2007.11.012

Wille, M., Kramers, J. D., Nägler, T. F., Beukes, N. J., Schröder, S., Meisel, Th, Lacassie, J. P. and Voegelin, A. R. (2007) Evidence for a gradual rise of oxygen between 2.6 and 2.5Ga from Mo isotopes and Re-PGE signatures in shales. *Geochimica et Cosmochimica Acta, 71*(10), 2417-2435. doi: 10.1016/j.gca.2007.02.019

Wille, M., Nagler, T. F., Lehmann, B., Schroder, S. and Kramers, J. D. (2008) Hydrogen sulphide release to surface waters at the Precambrian/Cambrian boundary. *Nature, 453*(7196), 767-769. doi: 10.1038/nature07072

Zhang, T., Shen, Y., Zhan, R., Shen, S. and Chen, X. (2009) Large perturbations of the carbon and sulfur cycle associated with the Late Ordovician mass extinction in South China. *Geology, 37*(4), 299-302. doi: 10.1130/g25477a.1

Zhang, T., Trela, W., Jiang, S. Y., Nielsen, J. K. and Shen, Y. (2011) Major oceanic redox condition change correlated with the rebound of marine animal diversity during the Late Ordovician. *Geology, 39*(7), 675-678. doi:10.1130/g32020.1

Zhou, L., Algeo, T. J., Shen, J., Hu, Z., Gong, H., Xie, S., Huang, J. and Gao, S. (2015) Changes in marine productivity and redox conditions during the Late Ordovician Hirnantian glaciation. *Palaeogeography, Palaeoclimatology, Palaeoecology, 420*, 223-234. doi: 10.1016/j.palaeo.2014.12.012

Zhou, L., Wignall, P. B., Su, J., Feng, Q., Xie, S., Zhao, L. and Huang, J. (2012) U/Mo ratios and $\delta^{98}/^{95}Mo$ as local and global redox proxies during mass extinction events. *Chemical Geology, 324-325*, 99-107. doi: 10.1016/j.chemgeo.2012.03.020

FIGURE CAPTIONS

Fig. 1. Carbonate carbon isotope, global sea level, and sea surface temperature variations during the Middle-Late Ordovician to Early Silurian. Global division of the geologic time scale is from Cohen et al. (2013). Carbonate carbon isotope curve is modified from Bergström et al. (2009) and Cramer et al. (2011). Global sea level curve is from Haq and Schutter (2008). Sea surface temperature curve is from Finnegan et al. (2011). HICE: Hirnantian Isotope Carbon Excursion; GICE: Guttenberg Isotope Carbon Excursion.

Fig. 2. Simplified map of the Siljan ring district showing recent drill sites. Map modified from Ebbestad and Hö gströ m (2007).

Fig. 3. Late Ordovician to Early Silurian stratigraphy in the Siljan ring district, central Sweden. Global division of the geologic time scale is from Cohen et al. (2013). Stage slices are based on Bergström et al. (2009) and Cramer et al. (2011). Regional stages are from Nõlvak et al. (2006) and Ebbestad et al. (2014). Stratigraphic succession of the Siljan ring district is based on Ebbestad and Hö gströ m (2007), Ebbestad et al. (2014), and Kröger et al. (2016). The U-Pb zircon ages of the Osmundsberget K-bentonite and Kinnekulle K-bentonite are from Bergström et al. (2008) and Bauert et al. (2014), respectively. Drill core names and arrows on the right side indicate the stratigraphic layers sampled.

Fig. 4. Geochemical profiles through three drillholes (Mora 001, Solberga #1, and Stumsnäs #1). Stratigraphic columns and formation names of each drillcore are modified from Lehnert et al. (2012, 2013). The error bars in the δ^{98}Mo and δ^{238}U profiles represent the long-term reproducibility of our secondary standards (0.11‰ and 0.09‰, respectively; 2SD). Vertical lines were added to the Fe_{HR}/Fe_T and Fe_{py}/Fe_{HR} columns to identify anoxic and euxinic conditions, respectively (details in Section 3.1). The sample depths in this figure are based on Lehnert et al. (2012, 2013). *J. Fm.= Jonstorp Formation; Sl. Lst.= Slandrom Limestone; Fj. S. = Fjäcka Shale; Fr. Fm.= Freberga Formation; S-S-F Lst.E= Skärlöv-Seby-Folkslunda Limestone equivalents; Se. Lst.= Segerstad Limestone; K. Lst.= Kullsberg Limestone; P. B. = Precambrian basement; O. beds = Obolus beds; "S-DF-CL" = shale + debris flow + compact limestone.*

Fig. 5. Diagram showing Fe_{py}/Fe_{HR} versus Fe_{HR}/Fe_T. Dashed lines are used to clarify different bottom water conditions (details in Section 3.1).

Fig. 6. Diagrams showing trace metal concentration versus TOC content; a) Mo vs TOC, b) U vs TOC, and c) Re vs TOC. Dashed lines in a) represent regression slopes for four modern anoxic basins reported by Algeo and Lyons (2006) (Saanich Inlet: 45 ± 5; Cariaco Basin: 25 ± 5; Framvaren Fjord: 9 ± 2; Black Sea: 4.5 ± 1; in mg/kg/wt.%). Solid trend lines of each trace metal vs TOC for the Fjäcka Shale are plotted with R^2 values (sample 135.01 is excluded when plotting the Re vs TOC trend line and calculating R^2 value because it is an obvious outlier).

Fig. 7. Diagrams showing: a) Mo EF versus U EF, b) Mo EF versus Re EF. Dashed lines in a) and b) represent the molar Mo/U (Algeo and Tribovillard, 2009) and Mo/Re (Crusius et al., 1996) ratios of modern seawater (1 × SW), respectively, and fractions of modern seawater (0.1 × SW, 0.3 × SW, and 3 × SW). Enrichment patterns and corresponding controls in a) are illustrated following Algeo and Tribovillard (2009). Re has similar behaviour as U (but Re generally has higher authigenic enrichments in ORM), suggesting the enrichment patterns and redox controls are broadly similar for Re and U (Morford and Emerson, 1999).

Fig. 8. Diagrams showing a) δ^{98}Mo versus Mo EF and b) δ^{238}U versus U EF. Dashed lines in a) and b) with R^2 values represent trend lines of δ^{98}Mo vs Mo and δ^{238}U vs U EF for each rock unit, respectively, where FS represents the Fjäcka Shale and KF represents the Kallholn Formation.

Fig. 9. Uranium isotope mass balance diagrams for A) the modern ocean and B) the late Katian ocean, and associated estimates of the anoxic/euxinic sink. Assumptions and calculation methods are described in the text.

Figure 1

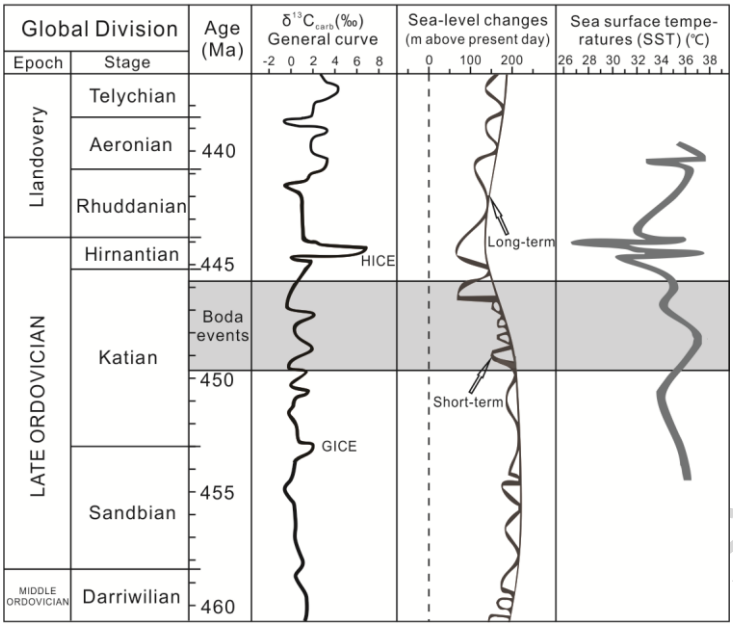

Figure 2

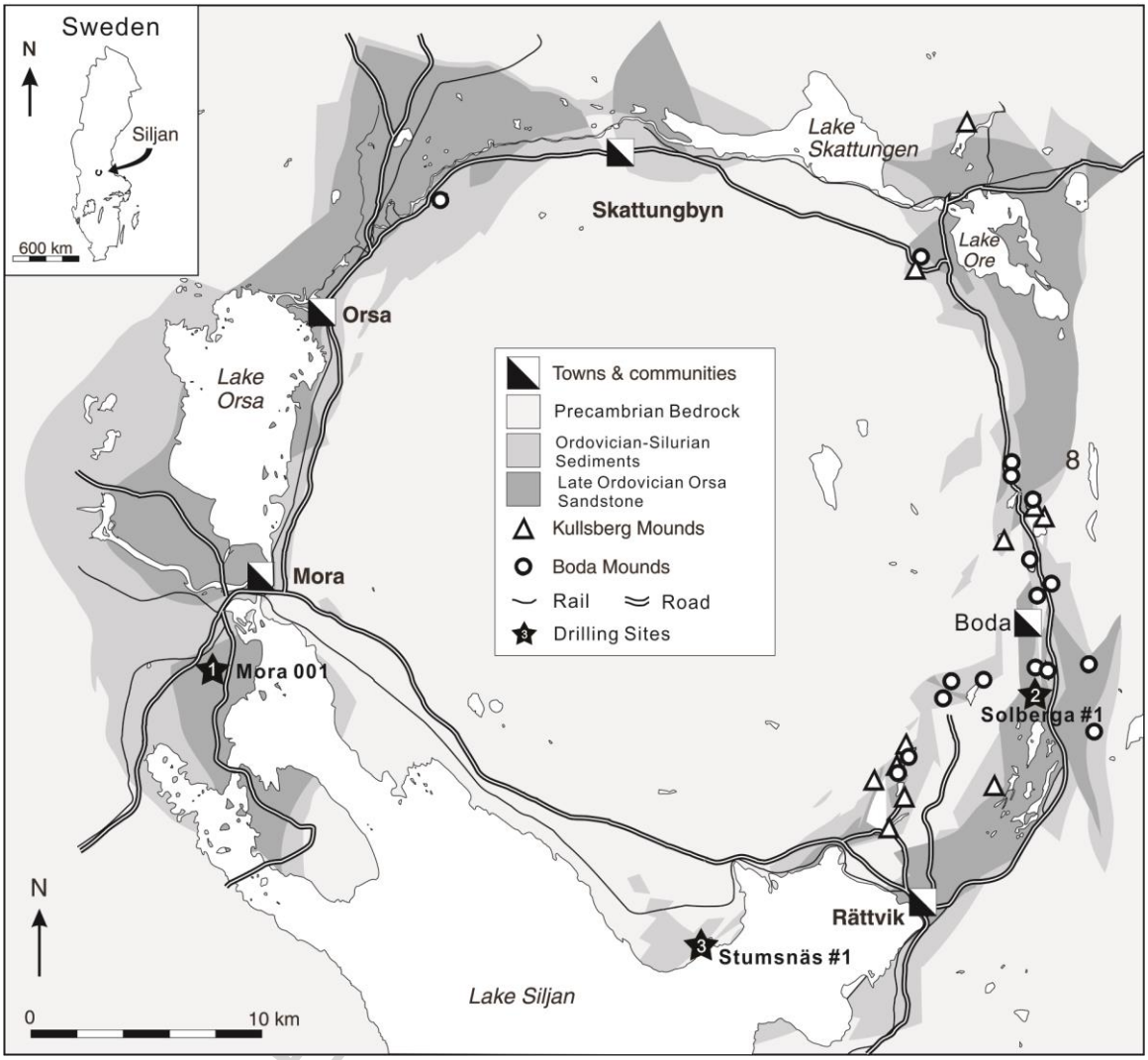

Figure 3

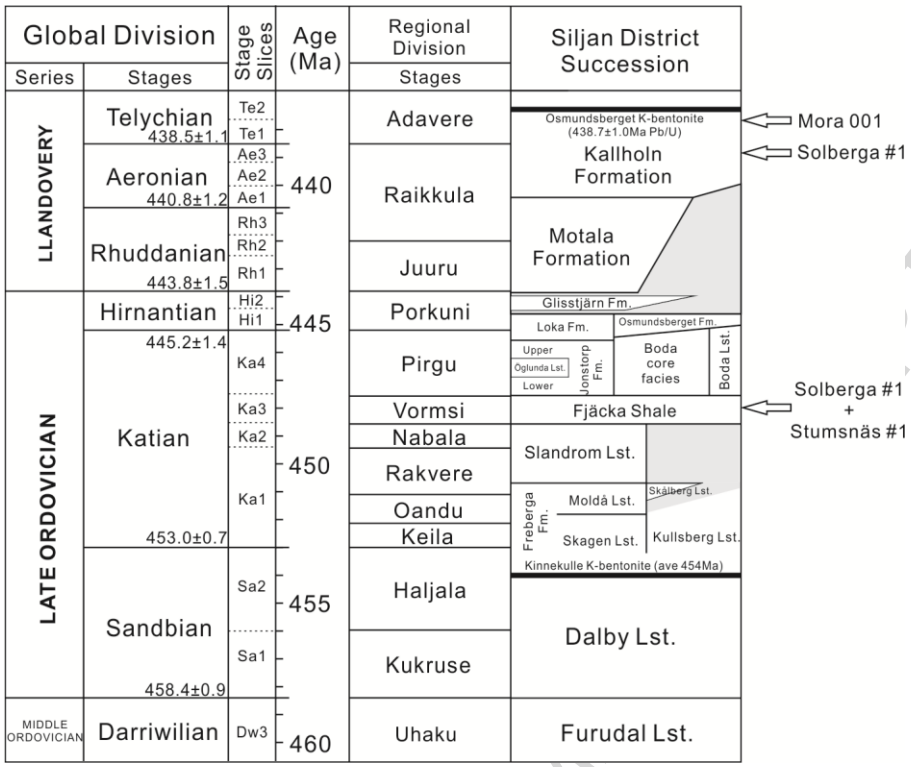

Figure 4

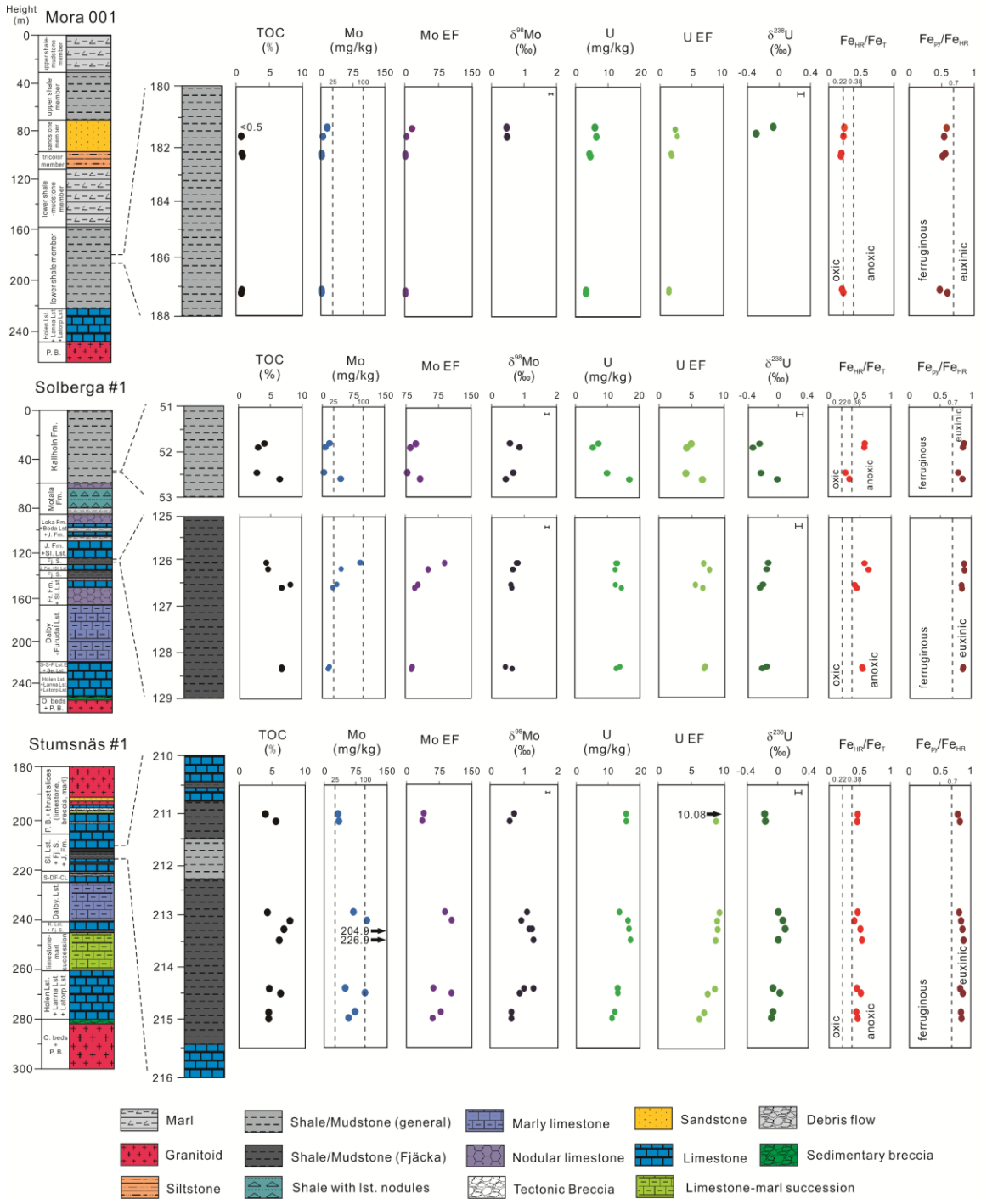

Figure 5

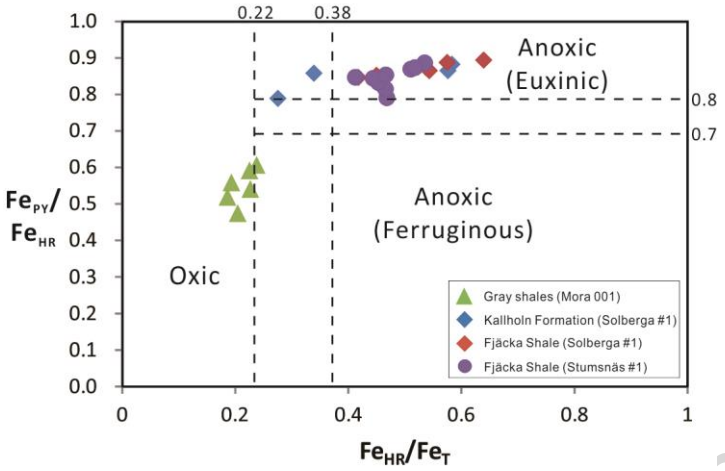

Figure 6

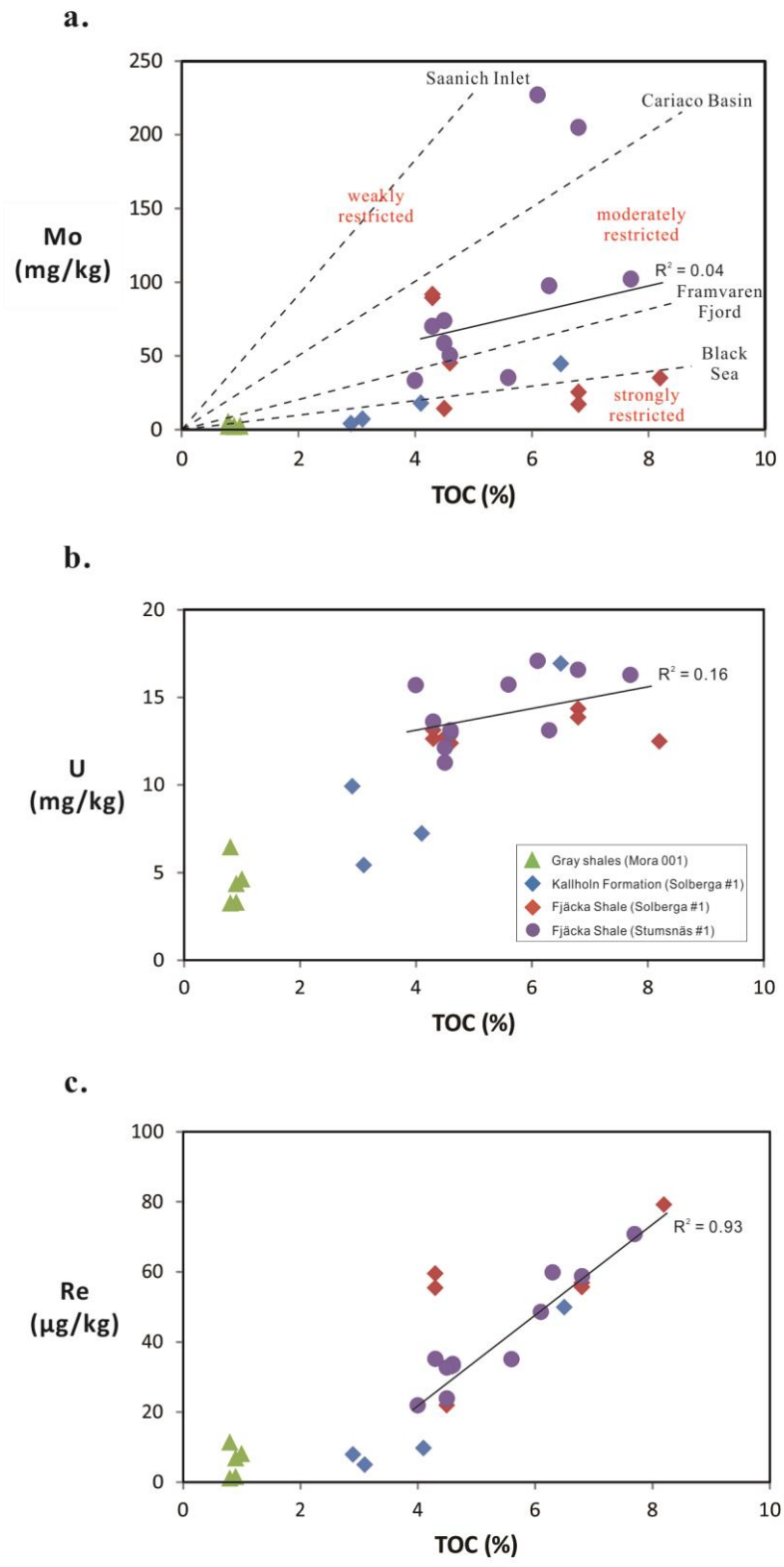

Figure 7

a.

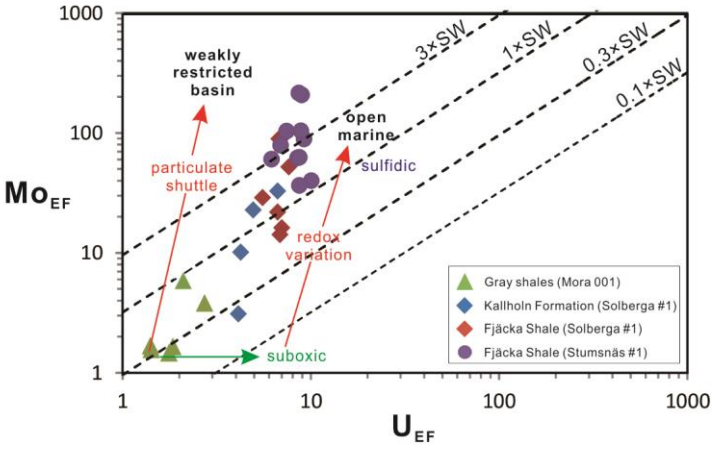

b.

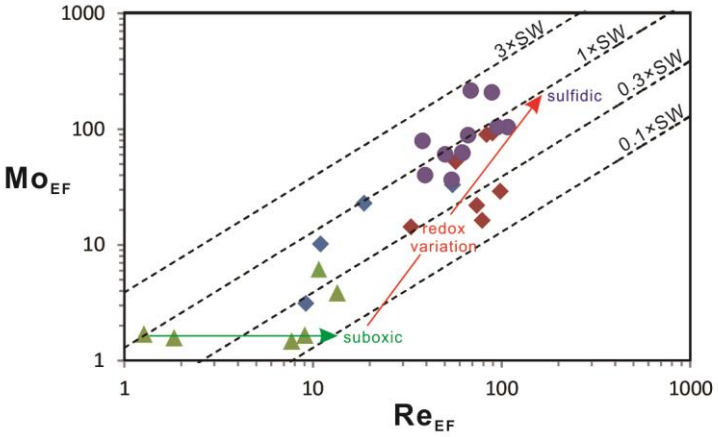

Figure 8

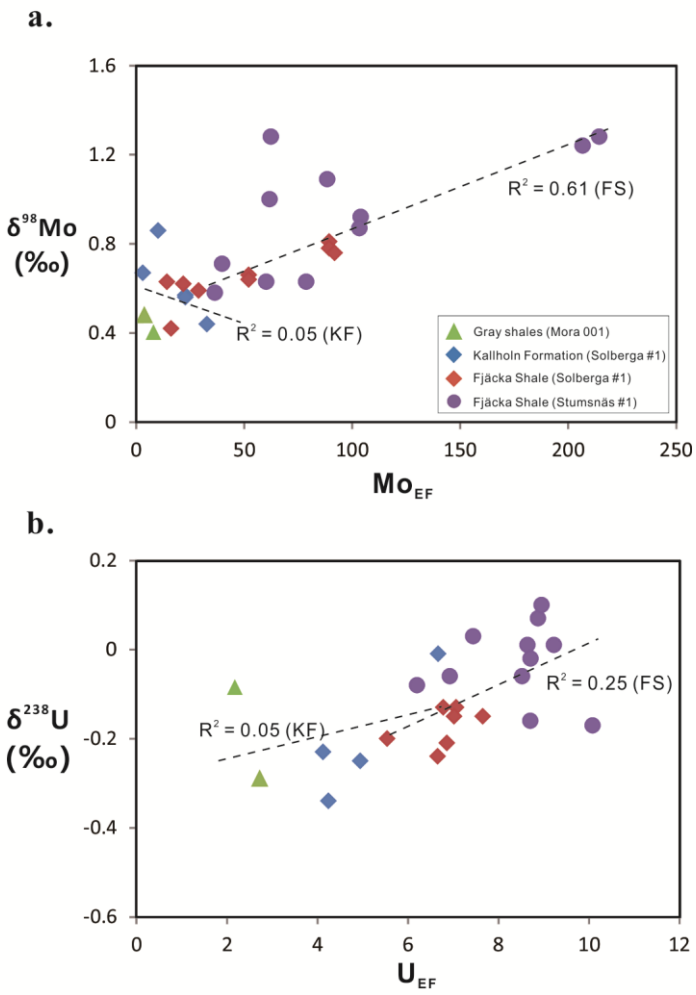

Figure 9

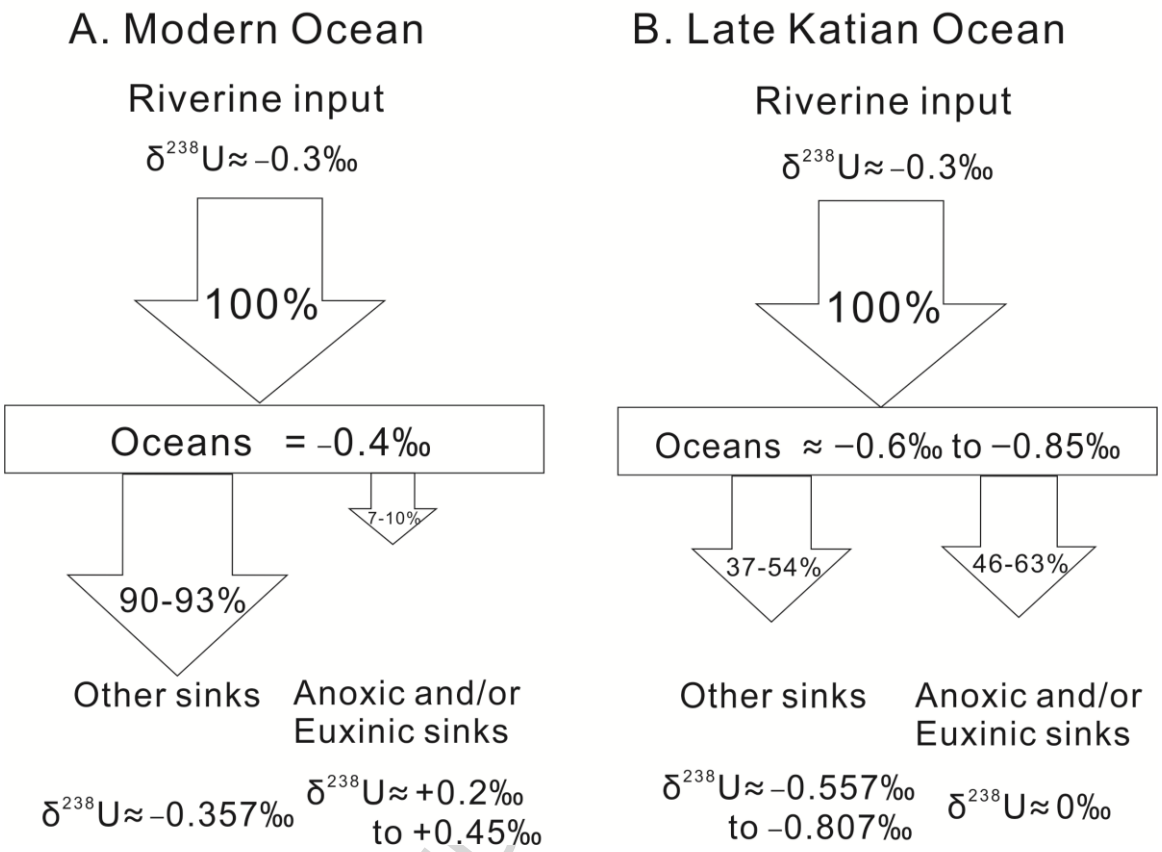

Table 1. Geochemical data for shales from the Mora 001, Solberga #1, and Stumsnäs #1 drillholes in Siljan district, central Sweden.

Sample	TOC[a] (wt.%)	Al (wt.%)	U (mg/kg)	Mo (mg/kg)	Re (µg/kg)	Mo/TOC (mg/kg/%)	U EF[b]	Mo EF[b]	Re EF[b]	δ^{238}U[c] (‰)	2SD Measured	2SD Reported	ne	δ^{98}Mo[f] (‰)	2SD Measured	2SD Reported	ne	Fe Carb[g] (wt.%)	Fe Ox (wt.%)	Fe Mag (wt.%)	Fe PY (wt.%)	Fe HR[h] (wt.%)	Fe HR/Fe T (wt.%)	Fe PY/Fe HR
Mora 001 - Gray shales (upper Kallholn Fm. Equivalent)																								
181.64	<0.05	7.0	5.3	7.4	8.9	N/A	2.2	5.7	10.3	-0.07	0.006	0.09	3	0.40	0.02	0.11	3	0.17	0.09	0.12	0.57	0.95	3.98	0.24	0.60
181.74	0.48	6.8	6.4	4.8	11.4	6.0	2.7	3.8	13.4	-0.29	0.12	0.12	3	0.48	0.02	0.11	3	0.17	0.08	0.11	0.43	0.80	3.52	0.23	0.54
182.34	0.49	7.1	4.3	1.9	6.8	2.1	1.8	1.5	7.7									0.15	0.07	0.10	0.40	0.73	3.76	0.19	0.56
182.42	1.0	7.2	4.6	2.2	8.1	2.2	1.8	1.6	9.1									0.16	0.08	0.10	0.37	0.71	3.81	0.19	0.52
187.10	0.09	6.6	3.3	1.9	1.5	2.1	1.4	1.6	1.8									0.16	0.09	0.11	0.33	0.70	3.43	0.20	0.47
187.20	0.08	6.6	3.2	2.1	1.0	2.6	1.4	1.7	1.3									0.15	0.08	0.09	0.46	0.78	3.45	0.23	0.59
Solberga #1 - Kallholn Fm.																								
60.81	4.1	4.2	7.2	17.8	9.8	4.3	4.9	22.7	18.7	-0.2	0.05	0.09	3	0.57	0.10	0.11	3	0.13	0.05	0.04	1.70	1.93	3.31	0.58	0.88

5																														
60.81rpt													3	0.56	0.04	0.113														
60.90	3.17	3.54	6.90	5.0	2.22	4.2	10.1	11.0	-0.34	0.006	0.09	3	0.86	0.05	0.113		0.115	0.015	0.048	1.488	2.56	0.58	0.86							
61.46	2.69	6.99	9.99	4.40	7.9	1.44	4.1	3.1	-0.23	0.005	0.09	3	0.67	0.00	0.113		0.108	0.006	0.055	0.708	3.21	0.28	0.79							
61.606	6.65	7.33	16.99	44.46	49.9	6.69	6.7	32.7	-0.01	0.015	0.15	3	0.44	0.03	0.113		0.106	0.005	0.044	0.944	1.10	3.23	0.34	0.86						
Solberga #1 - the Fjäcka Shale																														
135.01	4.43	5.34	12.46	89.92	55.5	20.88	6.8	89.4	83.4	-0.13	0.007	0.09	3	0.81	0.03	0.113		0.14	0.006	0.066	1.999	2.25	3.91	0.57	0.89						
135.01rpt1										-0.14	0.008	0.09	3	0.78	0.08	0.113														
135.01rpt2	4.43	5.33	13.11	91.15	59.5	21.13	7.1	91.9	89.7					0.76	0.03	0.113							4.10							
135.1566	4.36	4.66	12.44	45.41	33.0	9.98	7.7	52.1	57.2	-0.15	0.004	0.09	3	0.66	0.01	0.113		0.16	0.007	0.066	2.377	2.66	4.16	0.64	0.89					
135.15rpt													3	0.64	0.01	0.113														
13	8.0	6.0	12.4	34.0	79.0	4.22	5.0	28.0	98.0	-0.0	0.00	0.0	3	0.40	0.00	0.03		0.0	0.0	0.0	1.0	1.0	3.0	0.0	0.0					

5.49	2	5	.5	.8	.2		5	.9	.4	.20	3	09		59	5	11		12	06	06	33	58	77	42	85
135.56	6	6	14	25	56		6	21	74	-0.24		0.09	3	0.62	0.01	0.11	3	0.12	0.06	0.06	1.37	1.61	3.58	0.45	0.85
137.31	6	5	13	17	55		7	16	78	-0.15		0.09	3	0.42	0.04	0.11	3	0.13	0.06	0.05	1.65	1.90	3.52	0.54	0.87
137.35	4	5	12	14	21		6	14	33	-0.21		0.09	3	0.63	0.03	0.11	3	0.14	0.06	0.06	1.72	2.00	3.67	0.54	0.86
Stumsnäs #1 - the Fjäcka Shale																													
217.55	4	4	15	33	21		10	39	39	-0.17		0.09	3	0.71	0.03	0.11	3	0.14	0.08	0.09	1.17	1.48	3.17	0.47	0.79
217.69	5	5	15	35	35		8	36	54	-0.16		0.04	3	0.58	0.04	0.11	3	0.12	0.07	0.07	1.26	1.52	3.31	0.46	0.83
219.42	4	4	13	69	35	16.63	19.2	86	60	-0.01		0.09	3	1.09	0.08	0.11	3	0.11	0.06	0.06	0.98	1.20	2.58	0.47	0.81
219.58	7	5	16	102	70	13.73	18	103	08	-0.07		0.09	3	0.92	0.05	0.11	3	0.09	0.05	0.05	0.04	1.23	2.99	0.41	0.85
219.74	6	5	16	204	58	30.01	9.0	206	88	-0.10		0.09	3	1.24	0.03	0.11	3	0.11	0.06	0.05	0.49	1.72	3.36	0.51	0.87
219.74rpt													3	1.161	0.04	0.11	2								
219.99	6	5	17	226.	48	37.26	8.6	214.	68	-0.01		0.09	3	0.28	0.05	0.11	3	0.10	0.06	0.05	0.65	1.86	4.67	0.54	0.89

5				9				4																			
2											-0																
2			13	50	33			61	62		.0	0.0	.0		1.0		0.0		.11		0.10	0.06	0.05	1.04	1.25	2.75	0.45	0.83
0.87	4.6	4.4	.0	.3	.7	0.9	.5	.8	.1		.06		.09	3	.00		.01	3										
2																											
2											-0																
0.87rpt	4.6	4.3	13.1	50.3	33.3	10.9	8.7	62.4	61.9		.02	0.03	.09	3	1.28		0.07	3	.11							2.59		
2								10													0.10	0.06	0.05	1.37	1.57			
2			13	97	59			03	95	0		0.0	.0		0.0		0.0		.11		09	5	6	7	7	3.04	0.52	0.87
0.96	6.3	5.1	.1	.6	.8	5.5	.4	.4	.1		.03	0.04	.09	3	.87		.03	3										
2											-0										0.10	0.06	0.05	1.20	1.42			
2			12	73	23			78	38		.0	0.0	.0		0.0		0.0		.11							3.19	0.44	0.84
1.32	4.5	5.0	.1	.9	.8	16.4	.9	.8	.1		.06	0.06	.09	3	.63		.01	3										
2											-0										0.10	0.06	0.05	1.25	1.47			
2			11	58	32			60	00		.0	0.1	.1		0.6		0.0		.11							3.15	0.47	0.85
1.44	4.5	5.2	.3	.5	.7	3.0	.2	.2	.4		.08	1.1	.1	3	.63		.03	3										

[a] TOC = total organic carbon

[b] EF = enrichment factor = $(metal / Al)_{sample} / (metal / Al)_{ave.\ upper\ crust}$. Average upper crust metal values are from McLennan (2001) except for Re (Selby et al., 2007).

[c] U isotope data reported relative to CRM 145.

[d] Reported uncertainty is the 2SD of replicate measurements or 0.09‰, whichever is greater.

[e] Number of MC-ICP-MS analyses of the same sample solution.

[f] Mo isotope data reported relative to NIST SRM 3134 = +0.25‰.

[g] Reported uncertainty is the 2SD of replicate measurements or 0.11‰, whichever is greater.

[h] Fe_{HR} = highly reactive iron = carbonate iron (Fe_{Carb}) + ferric-oxide iron (Fe_{Ox}) + magnetite iron (Fe_{Mag}) + pyrite iron (Fe_{PY}).

[i] Fe_T = total iron

Table 2. Comparison of geochemical data among rock units from each drill core (ave = average)

Formations	TOC (wt.%)		U (mg/kg)		Mo (mg/kg)		Re (µg/kg)		U EF		Mo EF		Re EF		Mo/TOC (mg/kg/wt.%)		$\delta^{238}U$ (‰)		$\delta^{98}Mo$ (‰)		Fe_{HR}/Fe_T		Fe_{PY}/Fe_{HR}	
	ave	1SD	ave	1SD	ave	1SD	ave	1SD	ave	1SD	ave	1SD	ave	1SD	ave	1SD	ave	1SD	ave	1SD	ave	1SD	ave	1SD
Gray shale (equivalent to upper Kallholn Formation) (Mora 001)	0.9	0.1	4.5	1.2	3.4	2.3	6.3	4.2	1.9	0.5	2.6	1.7	7.3	4.8	3.0	1.7	-0.2	0.16	0.44	0.06	0.21	0.02	0.55	0.05
Kallholn Formation (Solberga #1)	4.2	1.7	9.9	5.1	18.3	18.5	18.1	21.3	5.0	1.2	17.2	13.2	23.5	21.5	3.7	2.4	-0.2	0.14	0.63	0.18	0.44	0.16	0.85	0.04
Fjäcka Shale (Solberga #1)	5.9	1.6	13.1	0.8	37.8	28.2	50.7	20.3	6.8	0.7	37.3	29.5	71.3	23.2	7.4	7.2	-0.2	0.04	0.62	0.12	0.53	0.08	0.87	0.02
Fjäcka Shale (Stumsnäs #1)	5.4	1.2	14.4	2.1	95.3	67.8	42.0	16.5	8.4	1.2	99.4	63.0	67.2	23.6	16.7	9.7	-0	0.09	0.91	0.26	0.47	0.04	0.84	0.03
Fjäcka Shale (all)	5.6	1.4	13.9	1.8	73.7	62.0	45.3	17.9	7.8	1.3	76.1	60.3	68.7	22.8	13.2	9.7	-0.1	0.11	0.80	0.26	0.49	0.06	0.85	0.03

Table 3. Authigenic U isotope compositions of the Fjäcka Shale

Sample	Al (wt.%)	U (mg/kg)	$\delta^{238}U$ [a] (‰)	2SD Measured	2SD [b] Reported	n [c]	$\delta^{238}U_{aut}$ [d,h] (‰) $\delta^{238}U_{det}$ [e] = -0.3‰	f_{auth} [f] (%)	f_{det} [g] (%)	$\delta^{238}U_{aut}$ [d,h] (‰) $\delta^{238}U_{det}$ [e] = -0.8‰	f_{auth} [f] (%)	f_{det} [g] (%)
Solberga #1												
135.01	5.35	12.6	-0.13	0.07	0.09	3	-0.10	0.85	0.15	-0.01	0.85	0.15
135.01rpt [h]	5.35	12.6	-0.14	0.08	0.09	3	-0.11	0.85	0.15	-0.03	0.85	0.15
135.15	4.65	12.4	-0.15	0.04	0.09	3	-0.13	0.87	0.13	-0.05	0.87	0.13
135.49	6.47	12.5	-0.20	0.03	0.09	3	-0.18	0.82	0.18	-0.07	0.82	0.18
135.56	6.19	14.3	-0.24	0.07	0.09	3	-0.23	0.85	0.15	-0.14	0.85	0.15
137.31	5.67	13.9	-0.15	0.02	0.09	3	-0.13	0.86	0.14	-0.04	0.86	0.14
137.35	5.32	12.7	-0.21	0.06	0.09	3	-0.19	0.85	0.15	-0.11	0.85	0.15
Stumsnäs #1												
217.55	4.47	15.7	-0.17	0.09	0.09	3	-0.16	0.90	0.10	-0.10	0.90	0.10
217.69	5.19	15.7	-0.16	0.04	0.09	3	-0.14	0.89	0.11	-0.08	0.89	0.11
219.42	4.23	13.6	0.01	0.05	0.09	3	0.05	0.89	0.11	0.11	0.89	0.11
219.58	5.26	16.3	0.07	0.04	0.09	3	0.12	0.89	0.11	0.18	0.89	0.11
219.74	5.31	16.6	0.10	0.03	0.09	3	0.15	0.89	0.11	0.21	0.89	0.11
219.95	5.67	17.1	0.01	0.03	0.09	3	0.05	0.88	0.12	0.12	0.88	0.12
220.87	4.37	13.0	-0.06	0.06	0.09	3	-0.03	0.88	0.12	0.04	0.88	0.12
220.87rpt	4.32	13.1	-0.02	0.03	0.09	3	0.02	0.89	0.11	0.08	0.89	0.11
220.96	5.06	13.1	0.03	0.04	0.09	3	0.08	0.87	0.13	0.16	0.87	0.13
221.32	5.03	12.1	-0.06	0.06	0.09	3	-0.02	0.86	0.14	0.06	0.86	0.14
221.44	5.21	11.3	-0.08	0.11	0.11	3	-0.04	0.84	0.16	0.06	0.84	0.16

[a] = U isotope date reported relative to CRM145
[b] = Reported uncertainty is the 2SD of replicate measurements or 0.09‰, whichever is greater
[c] = Number of MC-ICP-MS analyses of the same sample solution
[d] = Authigenic U isotope composition
[e] = Detrital U isotope composition
[f] = Fractions of authigenic U in the sample
[g] = Fractions of detrital U in the sample
[h] = Only U isotope data is reanalyzed for this sample

Table 4. Modeled U fluxes and isotopic compositions in modern ocean

Source		Flux (10^6 mol/yr)	$\delta^{238}U$ (‰)	$\Delta_{source-SW}$ (‰)	$\Delta_{source-SW}$ (‰) used in model	$\delta^{238}U$ (‰) used in model
River		42	−0.24 to −0.34	~ +0.10	+0.10	−0.30
Modern seawater		-	−0.40	-	-	−0.40
Sink		**Flux (10^6 mol/yr)**	**$\delta^{238}U$ (‰)**	**$\Delta_{sink-SW}$ (‰)**	**$\Delta_{sink-SW}$ (‰) used in model**	**$\delta^{238}U$ (‰) used in model**
Oxic	Coastal retention	7.6	−0.64	−0.24		
	Pelagic clay	3.0	−0.36	+0.04		
	Oceanic crust alteration (HT)	2.0	−0.40	0		
	Oceanic crust alteration (LT)	3.8	−0.15	+0.25	+0.043	−0.357
	Fe-Mn oxides	1.0	−0.64	−0.24		
	Carbonates	5.6	−0.20 to 0	+0.20 to +0.40		
Suboxic	Continental margin	15.3	−0.30	+0.10		
Anoxic	Anoxic/euxinic sediments	4.5	+0.20	+0.60	+0.60 to +0.85	+0.20 to +0.45

Data come from Andersen et al. (2014, 2016),Tissot and Dauphas (2015), Wang et al. (2016), Noordmann et al. (2016) and reference therein. SW = seawater; HT = high temperature; LT = low temperature.

Table. 5 Estimates for proportions of anoxic/euxinic sink in different geological times by U isotope mass balance model

Period	Age (Ma)	Lithology	$\delta^{238}U$ of anoxic/euxinic sink (‰)	$\delta^{238}U$ of seawater (‰)	Proportion of anoxic/euxinic sink (%)
Modern ocean [1]	0	N/A	+0.20 to +0.45	−0.40 [2]	7 to 10
OAE2 [3]	93	shale	−0.03[6]	−0.88 to −0.63	52 to 67
Late Permian [4]	252	carbonate	−0.05 to +0.20	−0.65	38 to 55
Late Katian [1]	448	shale	0	−0.85 to −0.60	46 to 63
Late Ediacaran [5]	560 to 551	shale	+0.29[6]	−0.56 to −0.31	0 to 27

[1] This study
[2] Stirling et al. (2007); Weyer et al. (2008); Andersen et al. (2015, 2016); Tissot and Dauphas (2015); Noordmann et al. (2016)
[3] Montoya-Pino et al. (2010)
[4] Brennecka et al. (2011a)
[5] Kendall et al. (2015)
[6] Authigenic average U isotope is recalculated in this study by using the equation in Section 5.2.2